New constraints on the active tectonic deformation of the Aegean

Marleen Nyst[1] and Wayne Thatcher
U.S. Geological Survey, Menlo Park, California, USA

Received 7 October 2003; revised 17 June 2004; accepted 26 July 2004; published 24 November 2004.

[1] Site velocities from six separate Global Positioning System (GPS) networks comprising 374 stations have been referred to a single common Eurasia-fixed reference frame to map the velocity distribution over the entire Aegean. We use the GPS velocity field to identify deforming regions, rigid elements, and potential microplate boundaries, and build upon previous work by others to initially specify rigid elements in central Greece, the South Aegean, Anatolia, and the Sea of Marmara. We apply an iterative approach, tentatively defining microplate boundaries, determining best fit rigid rotations, examining misfit patterns, and revising the boundaries to achieve a better match between model and data. Short-term seismic cycle effects are minor contaminants of the data that we remove when necessary to isolate the long-term kinematics. We find that present day Aegean deformation is due to the relative motions of four microplates and straining in several isolated zones internal to them. The RMS misfit of model to data is about 2-sigma, very good when compared to the typical match between coseismic fault models and GPS data. The simplicity of the microplate description of the deformation and its good fit to the GPS data are surprising and were not anticipated by previous work, which had suggested either many rigid elements or broad deforming zones that comprise much of the Aegean region. The isolated deforming zones are also unexpected and cannot be explained by the kinematics of the microplate motions. Strain rates within internally deforming zones are extensional and range from 30 to 50 nanostrain/year (nstrain/year, 10^{-9}/year), 1 to 2 orders of magnitude lower than rates observed across the major microplate boundaries. Lower strain rates may exist elsewhere within the microplates but are only resolved in Anatolia, where extension of 13 ± 4 nstrain/year is required by the data. Our results suggest that despite the detailed complexity of active continental deformation revealed by seismicity, active faulting, fault geomorphology, and earthquake fault plane solutions, continental tectonics, at least in the Aegean, is to first order very similar to global plate tectonics and obeys the same simple kinematic rules. Although the widespread distribution of Aegean seismicity and active faulting might suggest a rather spatially homogeneous seismic hazard, the focusing of deformation near microplate boundaries implies the highest hazard is comparably localized. *INDEX TERMS:* 8107 Tectonophysics: Continental neotectonics; 9335 Information Related to Geographic Region: Europe; 1206 Geodesy and Gravity: Crustal movements—interplate (8155); 1208 Geodesy and Gravity: Crustal movements—intraplate (8110); 8150 Tectonophysics: Plate boundary—general (3040); *KEYWORDS:* Aegean, continental deformation, GPS, neotectonics, microplate

Citation: Nyst, M., and W. Thatcher (2004), New constraints on the active tectonic deformation of the Aegean, *J. Geophys. Res.*, *109*, B11406, doi:10.1029/2003JB002830.

1. Introduction

[2] How continents deform has been hotly debated without definitive resolution since the earliest days of the development of the plate tectonic model [*Atwater*, 1970; *Molnar and Tapponnier*, 1975; *McKenzie*, 1977; *Molnar*, 1988; *England and Jackson*, 1989; *Gordon and Stein*, 1992; *Thatcher*, 1995, 2003]. The evident wide distribution of seismicity, active faulting, and tectonically generated topography have suggested that active continental deformation takes place over broad regions and differs fundamentally from the narrowly focused straining occurring between plates of oceanic lithosphere. End-member models have postulated this deformation is either quasicontinuous or due to the relative motions of a small number of rigid blocks or microplates (in this paper we use these terms interchangeably).

[1]Now at Department of Geophysics, Stanford University, Stanford, California, USA.

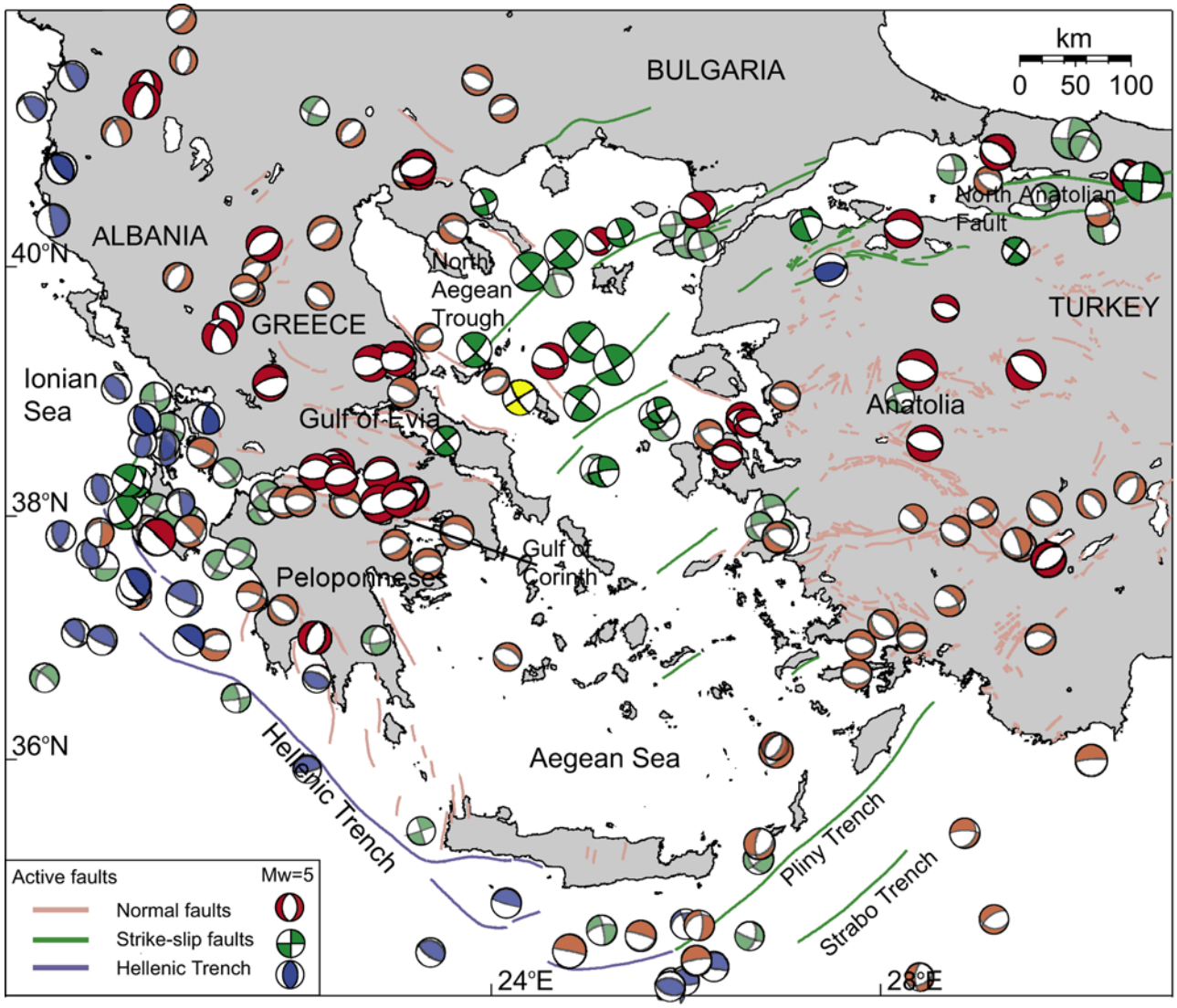

Figure 1. Aegean region, showing active faults and earthquake fault plane solutions. Geographic regions discussed in the text are shown for reference (from *Taymaz et al.* [1991], *Jackson et al.* [1992] (and references therein), *Baker et al.* [1997], and Harvard centroid moment tensor solutions). Geographic regions discussed in the text are shown for reference. Body wave inversion solutions are shown in bright red, blue, and green, others are fainter. The 2001 M = 6.4 Skyros earthquake, discussed in section 3 (at approximately 24.5°E, 39°N), is indicated in yellow.

[3] The absence of precise quantitative measures of regional continental deformation has been the chief obstacle in determining which, if either, description is correct. However, GPS methods have the singular capability of providing the necessary quantification, permitting accurate mappings of site velocities across deforming zones in a common reference frame [e.g., *Segall and Davis*, 1997]. GPS mappings are therefore increasingly being applied to define patterns of movement [e.g., *Beavan et al.*, 1999; *Bennett et al.*, 1998; *McClusky et al.*, 2000; *Sagiya et al.*, 2000; *Thatcher et al.*, 1999; *Wang et al.*, 2001]. Newer work is beginning to relate these kinematic patterns to the forces that drive and resist continental deformation [e.g., *Flesch et al.*, 2000, 2001].

[4] High levels of seismicity and abundant evidence of active tectonic deformation have long encouraged study of the Aegean region to understand the implications of plate tectonics for continental deformation. Studies done in the ~20 years following acceptance of the plate tectonic theory have used seismologic data, active fault distributions, and seafloor bathymetry to define the major tectonic boundaries of the Aegean and infer the magnitude and sense of relative motions across them [*McKenzie*, 1972, 1978; *Le Pichon and Angelier*, 1979, 1981; *McKenzie and Jackson*, 1983; *Taymaz et al.*, 1991]. This work used plate tectonic concepts to demonstrate the westward motion of a stable Anatolian block and northward underthrusting of the African plate beneath the Aegean Sea and seismologic data to determine the style and distribution of earthquake faulting.

[5] Figure 1 shows the close spatial relation between earthquake faulting parameters determined from seismic wave studies and the distribution and sense of motion on

Table 1. Information on GPS Networks and Data Collection[a]

Data	Survey Years	Number of Sites	RMS S/N Ratio	Source
Aegean	88 (s)–89 (n)–92–96	61	11.58	*McClusky et al.* [2000] (and references therein)
West Hellenic Arc	93–94–96	61	11.58	*McClusky et al.* [2000] (and references therein)
Anatolia	91 (e)–92 (w)–93 (e)–94–95–96	61	11.58	*McClusky et al.* [2000] (and references therein)
Marmara	90–92–94–96	61	11.58	*McClusky et al.* [2000] (and references therein)
Central Greece	89–91–93–95 (Corinth)–96 (Corinth)–97 (Evia)	63	18.21	*Clarke et al.* [1998]
West Hellenic Arc	93–94–95 (f)–96–97 (f)–98	34	29.46	*Cocard et al.* [1999]
Bulgaria	94 (f)–96–97 (f)–98	4	2.23	*Kotzev et al.* [2001]
Western Anatolia	92–93 (w)–94–95 (w)–96–97 (w)–98–99 (m)	136	35.36[b]	*Ayhan et al.* [2002]
Northwestern Anatolia	97–98–99	76	11.33	*Meade et al.* [2002]

[a]Abbreviations are as follows: s, south; n, north; e, east; w, west; f, few; m, Marmara. No indication means all stations were measured. RMS S/N ratio is computed from $1/N\sqrt{\sum_{i=1}^{N}(v_i/\sigma_i)^2}$, where N is the number of data, v is the velocity vector, and σ is the 1-sigma standard deviation of the velocity measurement.

[b]Data uncertainties are underestimated by factor of 2–5 (see text).

mapped active faults [*McKenzie*, 1972, 1978; *Le Pichon and Angelier*, 1981; *McKenzie and Jackson*, 1983; *Taymaz et al.*, 1991; *Goldsworthy et al.*, 2002]. Normal faulting (red fault plane solutions and fault traces) is widespread on mainland Greece and in western Turkey but rare elsewhere. Strike-slip faulting (green solutions and faults) is largely confined to the northern Aegean Sea and along the North Anatolian fault. Reverse faulting (blue) occurs near the Hellenic Trench, in the Ionian Sea off western Greece, and northwest into Albania. Extensional earthquake slip vectors (not shown in Figure 1) are generally perpendicular to normal faults, right lateral slip vectors are parallel to strike-slip faults, and reverse slip vectors are perpendicular to the Hellenic Trench, mapped thrust faults, or active fold axes. While studies such as these have illuminated many important features of Aegean tectonics, they have not led to development of a single widely accepted kinematic model of Aegean deformation.

[6] However, GPS survey results obtained in the past decade have begun to quantitatively fill in the patterns of contemporary Aegean deformation and provide crucial clues to the large-scale kinematics [*Billiris et al.*, 1991; *Le Pichon et al.*, 1995; *Davies et al.*, 1997: *Clarke et al.*, 1998; *Cocard et al.*, 1999; *Briole et al.*, 2000; *McClusky et al.*, 2000; *Kotzev et al.*, 2001*; Ayhan et al.*, 2002]. In particular, *Le Pichon et al.* [1995] used early GPS measurements to quantify clockwise rotation of central Greece and westward increasing extension across the Gulf of Corinth, and *McClusky et al.* [2000] used an extensive set of GPS data to define rigid blocks in central Anatolia and the southern Aegean. A number of recent studies have also used a dense GPS network in NW Anatolia to suggest the existence of an additional microplate sliver, the South Marmara block, in this region [*Meade et al.*, 2002; *Le Pichon et al.*, 2003; *Flerit et al.*, 2003].

[7] In this paper we present no new GPS data. Instead we merge the published results from six separate localized networks into a common reference frame and analyze the combined data set. Collectively, the networks provide a synoptic mapping of the Aegean velocity field relative to Eurasia that we use to define microplate motions and infer where deformation is localized.

[8] This paper is organized into six subsequent sections. We briefly describe the data and our analysis methods. We next present our four-microplate model and discuss its main features. We then examine the GPS evidence for the existence of an independent South Marmara microplate sliver. We go on to compare our model with kinematic descriptions of Aegean deformation proposed in previous studies, then compare and contrast our model of continental deformation with plate tectonics, and end with a summary and discussion.

2. Data and Analysis Methods

[9] GPS networks used here are listed in Table 1. Surveys were carried out as early as 1988 and as recently as 2001. No sites are known to have been affected by coseismic earthquake movements, although two stations on the north shore of the Gulf of Corinth may have been influenced by postseismic deformation from the 1995 $M = 6.2$ Aigeon earthquake [see *Clarke et al.*, 1998]. Site velocities in each case have been referred to an individually determined stable Eurasia reference frame that varies slightly from study to study. More details on each network, survey procedures, and analysis methods are contained in the original references cited in Table 1. The GPS velocities are listed in Table 2.

[10] Site velocities from each network have been combined into a single common reference frame using the largest and most widespread network (that of *McClusky et al.* [2000]) as the basis net. We applied a seven-parameter Helmert transformation using common stations between pairs of networks. Each network was compared with the *McClusky et al.* [2000] net by finding the transformation that minimized the root-mean-square (RMS) differences between velocities of common sites. Transformation parameters (scale, three rotations, and three translations) are listed in Table 3. Although velocities at a few common or nearby sites differ as much as 5 mm/yr, the average discrepancies are generally much smaller (see RMS misfit, Table 3). The GPS velocity field relative to a stable Eurasian reference frame is shown in Figure 2. The local and regional consistency among the GPS vectors demonstrates the reliability of the

Table 2. GPS Velocity Vectors, Uncertainties, Misfits to Best Euler Vectors[a]

Longitude, °E	Latitude, °N	v_{east}	v_{north}	σ_{east}	σ_{north}	m_{east}	m_{north}	Euler Vector[b]
21.96	39.24	−4.69	−12.75	4	3.45	−3.48	−3.71	1
21.8	38.91	−7.44	−11.71	4.66	3.86	1.47	6.39	1
22.4	38.64	−9.81	−15.6	1.46	1.31	5.15	3.25	1
22.5	38.61	−10.08	−16.24	1.25	1.11	3.34	3.72	1
22.58	38.4	−11.86	−16.76	0.94	0.81	3.65	−2.82	1
20.67	39.73	−0.44	−4.4	1.2	1.1	−1.06	1.3	1
20.67	39.73	−0.4	−4.37	0.82	1	−1.21	0.33	1
20.88	39.46	−2.7	−5.76	1.23	1.5	−1.83	0.45	1
20.47	39.29	−4.12	−3.13	1.02	1.3	1.45	1.04	1
20.99	39.17	−5.21	−6.46	1.03	1.2	0.7	−0.12	1
21.17	38.86	−7.76	−7.61	0.93	1	2.35	2.07	1
21.29	38.7	−9.18	−8.42	1.12	1.4	2.26	−1.74	1
20.66	39.73	−0.44	−4.34	3.56	2.77	−4.39	0.55	1
22.86	38.62	−10.06	−18.57	1.57	1.32	2.08	−0.6	1
23.2	38.57	−10.55	−20.77	0.82	0.8	0.66	−2.99	1
22.79	38.53	−10.8	−18.12	1.15	1.01	−0.15	1.87	1
22.87	38.43	−11.66	−18.63	1.25	1.11	−0.84	−3.64	1
23.22	38.43	−11.74	−20.9	1.03	1.01	0.77	−1.7	1
22.86	38.26	−13.09	−18.57	1.25	1.11	0.29	0.3	1
23.03	38.25	−13.21	−19.67	0.94	0.81	−2.58	−2.35	1
23.37	38.99	−7.06	−21.87	0.82	0.81	−9.53	−0.79	1
23.34	38.78	−8.82	−21.67	0.83	0.71	−2.9	−0.24	1
23.46	38.84	−8.34	−22.45	0.82	0.81	−0.16	−2.01	1
23.67	39.15	−5.79	−23.8	4.02	2.84	−3.56	5.28	1*
27.42	37.03	−16.22	−28.77	1.3	1.3	1.52	3.47	2
26.93	36.75	−16.3	−28.53	1.2	1.1	−0.2	1.53	2
26.41	36.59	−16.28	−28.27	1.2	1.1	1.38	−2.23	2
26.21	35.13	−17.44	−28.17	1.3	1.1	1.64	−0.23	2
25.44	36.35	−16.2	−27.78	1.2	1.1	−0.2	−3.22	2
25.38	37.45	−15.26	−27.75	1.4	1.3	−1.34	1.35	2
24.69	35.4	−16.79	−27.4	1.2	1.1	0.29	0.5	2
24.52	36.75	−15.6	−27.31	1.2	1.1	−0.8	2.11	2
24.41	37.36	−15.05	−27.25	1.2	1.1	−2.55	1.05	2
24.07	34.84	−17.09	−27.08	3.1	3.2	0.99	0.88	2
23.93	35.33	−16.64	−27	1.3	1.1	0.04	2.3	2
23.3	35.87	−16	−26.67	1.02	1.2	−0.7	−2.76	2
24.08	35.49	−16.55	−27.08	1.51	1.91	2.05	−5.33	2
23.57	35.42	−16.46	−26.81	0.81	1	2.74	0.68	2
24.69	35.4	−16.78	−27.4	0.91	1	−0.58	1.78	2
26.3	35.31	−17.32	−28.21	1.91	2.1	4.78	−0.42	2
24.42	35.17	−16.9	−27.26	1.12	1.2	−0.15	5.4	2
24.07	34.84	−17.09	−27.08	0.71	0.8	−1.81	−0.48	2
24.39	38.09	−14.42	−27.24	1.1	1.1	−1.48	1.34	2
23.59	38.64	−13.72	−26.83	0.92	0.91	1.73	2.26	2
23.72	38.63	−13.76	−26.89	0.82	0.81	−1.3	1.61	2
24.11	38.66	−13.85	−27.1	0.93	0.81	−0.76	−0.67	2
23.74	38.43	−13.94	−26.9	1.34	1.21	−0.06	2.02	2
23.96	38.39	−14.04	−27.02	0.82	0.8	−0.81	−0.45	2
24.19	38.35	−14.14	−27.14	0.82	0.8	−0.36	−0.33	2
24.39	38.09	−14.42	−27.24	0.92	0.9	−0.97	−1.66	2
23.93	38.08	−14.3	−27	0.9	0.9	−1.4	−3.3	2
23.93	38.08	−14.3	−27.01	0.31	0.3	2.18	−0.91	2
23.54	38.45	−13.87	−26.8	0.93	0.81	−0.72	1.89	2
23.21	38.1	−14.07	−26.63	0.94	0.81	−2.77	0.12	2
23.35	38.21	−14.02	−26.7	1.13	1.1	0.24	−0.8	2
23.85	38.23	−14.15	−26.96	0.92	0.9	−4.53	−0.52	2
23.93	38.08	−14.3	−27	2.05	2.01	−0.99	1.03	2
23.44	38.07	−14.16	−26.75	4.01	2.98	−0.21	2.34	2
23.61	38.02	−14.26	−26.84	1.33	1.31	0.55	−0.3	2
23.94	37.82	−14.52	−27.01	1.13	1.1	−4.37	3.27	2
22.98	36.31	−15.54	−26.51	1.2	1.1	−0.16	0.91	2
22.82	37.18	−14.75	−26.42	1.2	1.1	−2.05	−1.98	2
22.95	36.72	−15.19	−26.49	0.61	0.7	0.17	1.69	2
22.98	36.31	−15.55	−26.51	1.03	1.1	−2.82	0.17	2
23.09	37.8	−14.3	−26.56	1.78	1.51	−1.73	−0.86	2
21.97	38.23	−13.61	−25.97	1.28	1.02	1.37	−3.73	2
22.19	38.13	−13.76	−26.09	1.26	1.11	−5.79	−11.47	2
22.64	38.01	−13.99	−26.33	0.83	0.8	−2.3	−3.39	2
21.95	38.07	−13.74	−25.96	1.37	1.21	−0.87	−0.44	2
22.43	37.85	−14.07	−26.21	1.26	1.11	−1.61	−4.62	2
21.88	36.79	−14.83	−25.92	1.2	1.1	−3.37	2.12	2

Table 2. (continued)

Longitude, °E	Latitude, °N	v_{east}	v_{north}	σ_{east}	σ_{north}	m_{east}	m_{north}	Euler Vector[b]
20.8	37.67	−13.77	−25.33	1.6	1.6	3.57	2.73	2
21.12	38.49	−13.14	−25.51	1.01	1.4	6.01	8.51	2
20.7	37.93	−13.52	−25.28	1.02	1.3	0.92	12.35	2
21.92	37.7	−14.05	−25.94	1.02	1.2	−5.7	−2.55	2
20.8	37.67	−13.77	−25.33	0.52	0.6	2.28	9.22	2
21.64	37.49	−14.16	−25.79	0.91	1.2	−9.47	−5.15	2
21.02	37.25	−14.2	−25.45	1.24	1.4	−1.89	5.53	2
21.83	37.24	−14.43	−25.9	0.92	1.1	−7.42	−1.13	2
22.39	37.03	−14.76	−26.19	1.12	1.4	−2.13	−3.99	2
21.88	36.79	−14.83	−25.92	0.62	0.7	−4.26	−0.53	2
22.41	36.47	−15.25	−26.2	1.21	1.61	−7.46	−0.16	2
21.88	36.79	−14.83	−25.92	0.84	0.8	−2.93	4.8	2
21.58	38.01	−13.69	−25.76	1.49	1.21	1.87	2.05	2
28.43	37.17	−16.41	−29.26	2	2	−0.49	7.96	2*
28.08	37.61	−15.94	−29.09	1.2	1.2	−3.36	8.89	2*
27.96	36.77	−16.6	−29.03	1.2	1.2	3	3.53	2*
27.84	37.2	−16.2	−28.97	1.4	1.4	0.2	3.37	2*
27.78	35.95	−17.22	−28.94	1.3	1.2	9.22	0.04	2*
27.39	36.68	−16.5	−28.75	1.4	1.4	7.5	−1.95	2*
27.22	35.49	−17.43	−28.67	1.3	1.1	5.93	−2.03	2*
26.99	37.78	−15.46	−28.56	1.2	1.1	−3.84	4.26	2*
26.39	38.31	−14.84	−28.26	1.2	1.2	−2.26	5.46	2*
26.08	38.44	−14.63	−28.1	1.2	1.1	−5.17	4.7	2*
27.08	38.02	−15.29	−28.6	0.6	0.6	−3.92	8.82	2*
26.72	38.43	−14.84	−28.42	0.3	0.3	−5.33	8.36	2*
26.38	38.31	−14.83	−28.25	0.3	0.3	−4.88	5.81	2*
24.54	38.89	−13.78	−27.32	1.2	1.1	1.18	3.32	2*
23.91	39.21	−13.32	−26.99	3.74	3.08	1.63	3.01	2*
24.54	38.89	−13.78	−27.32	0.92	0.81	1.54	0.23	2*
24.59	38.8	−13.88	−27.35	0.81	0.81	1.2	2.56	2*
23.13	38.02	−14.12	−26.58	3.72	3.52	−2.58	−8.2	2*
22.88	37.72	−14.31	−26.45	1.24	1.2	0.98	−4.23	2*
22.94	37.79	−14.26	−26.48	0.83	0.8	−1.11	−0.19	2*
38.22	38.46	−17.67	11.24	1.3	1.5	5.67	−0.34	3
37.96	39.45	−19.98	10.72	1.2	1.5	1.68	−0.82	3
36.07	37.39	−15.42	6.94	2.2	1.5	3.22	4.86	3
34.88	40.45	−22.54	4.56	1.5	1.5	5.94	0.24	3
34.81	39.8	−21.05	4.42	1.3	1.5	0.05	−0.02	3
34.8	39.11	−19.46	4.4	2	1.5	0.66	−2.2	3
34.55	36.9	−14.37	3.9	1.5	1.5	1.27	−0.1	3
33.19	37.38	−15.52	1.18	1.1	1.5	1.42	1.02	3
32.76	39.89	−21.31	0.32	1	1.5	0.51	−2.52	3
32.73	39.87	−21.26	0.26	1	1.5	0.46	−2.46	3
32.16	36.43	−13.32	−0.88	1.5	1.4	3.32	1.38	3
31.81	39.56	−20.54	−1.58	1.4	1.2	−0.06	−1.52	3
30.8	40.39	−22.42	−3.6	1.2	1.2	2.52	0.4	3
30.64	38.77	−18.69	−3.92	1.2	1.2	−2.91	0.72	3
30.64	39.66	−20.74	−3.92	1.5	1.4	−3.66	1.32	3
30.3	37.69	−16.18	−4.6	1.2	1.2	−3.32	−3.8	3
29.14	37.94	−16.69	−6.92	1.2	1.1	−4.81	−1.18	3
28.67	39.05	−19.21	−7.86	1.2	1.1	−1.69	1.06	3
28.48	38.31	−17.49	−8.24	1.5	1.4	−5.21	−4.36	3
28	38.25	−17.3	−9.2	1.4	1.4	−3.7	−4.3	3
27.87	39.01	−19.04	−9.46	1.2	1.2	−1.26	−1.44	3
27.59	39.29	−19.65	−10.02	2.5	2.6	3.75	−1.58	3
27.32	39.02	−19	−10.56	1.2	1.2	−1.9	−3.14	3
27.31	38.71	−18.29	−10.58	1.2	1.1	0.59	−4.42	3
27.11	39.24	−19.48	−10.98	2.6	2.6	1.08	−0.82	3
26.71	39.33	−19.64	−11.77	1.4	1.3	−0.46	1.17	3
26.7	39.31	−19.59	−11.79	1.2	1.2	1.09	−0.41	3
26.45	39.23	−19.37	−12.29	1.2	1.1	−1.13	−0.91	3
32.76	39.89	−21.31	0.32	0.15	0.15	−0.24	−1.84	3
31.81	39.56	−20.54	−1.58	0.32	0.45	−0.45	−1.49	3
30.8	40.39	−22.42	−3.6	0.62	0.75	2.97	0.48	3
30.64	38.77	−18.69	−3.92	0.32	0.45	−3.01	0.27	3
30.64	39.66	−20.74	−3.92	0.45	0.46	−3.77	0.42	3
30.52	40.35	−22.32	−4.16	0.3	0.31	5.11	−1.56	3
29.89	40.07	−21.64	−5.42	1.52	1.81	2.04	−0.06	3
29.78	38.73	−18.55	−5.64	0.3	0.3	−3.91	−0.91	3
29.42	39.04	−19.24	−6.36	0.3	0.3	−3.67	−0.45	3
29.25	39.33	−19.9	−6.7	0.3	0.3	−2.79	2.04	3

Table 2. (continued)

Longitude, °E	Latitude, °N	v_{east}	v_{north}	σ_{east}	σ_{north}	m_{east}	m_{north}	Euler Vector[b]
29.04	39.15	−19.47	−7.12	0.3	0.3	−3.29	1.18	3
28.96	39.42	−20.08	−7.28	0.3	0.3	−4.17	1.5	3
28.91	38.76	−18.56	−7.38	0.3	0.3	−4.96	−0.59	3
28.86	38.02	−16.85	−7.48	0.3	0.3	−5.45	−3.56	3
28.67	39.05	−19.21	−7.86	0.3	0.3	−3.09	0.53	3
28.63	39.61	−20.49	−7.94	0.3	0.3	−0.91	2.42	3
28.48	38.31	−17.49	−8.24	1.2	1.21	−6.66	−3.56	3
28.42	38.73	−18.45	−8.36	0.3	0.3	−4.8	−0.62	3
28.28	38.97	−18.99	−8.64	0.3	0.3	−4.44	0.12	3
28.24	38.03	−16.82	−8.72	0.3	0.3	−2.88	−3.04	3
28.14	39.23	−19.57	−8.92	0.3	0.3	−2.84	1.25	3
28	38.25	−17.3	−9.2	1.65	1.66	−3.76	−8.7	3
27.87	39.01	−19.04	−9.46	0.45	0.45	−1.93	−2.28	3
27.86	38.48	−17.82	−9.48	0.17	0.3	−1.33	−7.57	3
27.78	38.06	−16.84	−9.64	0.3	0.3	−3.98	−4.74	3
27.67	38.68	−18.26	−9.86	0.17	0.3	−1.37	−4.03	3
27.59	39.29	−19.65	−10.02	0.9	1.05	−2.78	−0.27	3
27.45	38.57	−17.98	−10.3	0.3	0.3	−5.31	−3.77	3
27.32	39.02	−19	−10.56	0.45	0.45	−1.68	−3.59	3
27.31	38.71	−18.29	−10.58	0.15	0.15	−0.18	−5.22	3
27.16	38.6	−18.02	−10.88	0.3	0.3	−4.63	−3.7	3
27.13	38.49	−17.76	−10.94	0.3	0.3	−4.78	−5.53	3
27.11	39.24	−19.48	−10.98	2.7	3.01	1.83	−1.41	3
26.88	39.01	−18.93	−11.44	0.9	1.05	−2.29	−0.02	3
26.71	39.33	−19.64	−11.77	1.05	1.35	−1.96	0.46	3
26.7	39.31	−19.59	−11.79	0.45	0.45	1.29	−0.52	3
32.76	39.89	−21.3	0.32	0.89	0.83	−0.88	−1.35	3
31.81	39.56	−20.55	−1.57	1.03	0.82	−0.32	−0.75	3
30.8	40.39	−22.41	−3.6	0.84	0.85	2.18	0.42	3
30.64	39.66	−20.73	−3.93	0.99	0.93	−3.94	2.14	3
28.67	39.05	−19.2	−7.86	0.79	0.73	−2.24	1.57	3
27.87	39.01	−19.03	−9.45	0.78	0.75	−1.79	−1.02	3
27.59	39.29	−19.66	−10.02	2.03	2.11	3.46	−1.34	3
27.32	39.02	−19.01	−10.57	0.86	0.78	−2.28	−2.54	3
27.11	39.24	−19.49	−10.97	2.09	2.18	0.61	−0.55	3
26.89	39.01	−18.93	−11.43	2.92	2.88	−0.33	1.04	3
26.71	39.33	−19.63	−11.78	0.97	0.93	−0.77	1.33	3
26.7	39.31	−19.59	−11.79	0.84	0.76	0.43	−0.03	3
26.45	39.23	−19.38	−12.29	1.2	1.09	−2.68	−1.66	3
30.61	36.83	−14.21	−3.98	1.4	1.4	4.11	−4.72	3*
29.65	36.19	−12.68	−5.9	1.4	1.2	1.58	−4.3	3*
29.44	36.72	−13.89	−6.32	1.5	1.4	0.49	−4.48	3*
27.49	37.82	−16.26	−10.22	1.4	1.4	−3.54	−8.68	3*
26.79	38.74	−18.29	−11.61	0.3	0.3	−3.1	−7.1	3*
28.92	39.93	−18.57	0.94	2.1	2	−5.29	−2	4
27.91	39.72	−17.54	−3.02	1.3	1.2	−4.36	−1.23	4
27.82	40.4	−20.83	−3.37	1.3	1.2	2.12	1.86	4
27.76	40.06	−19.18	−3.61	1.9	1.9	−4.11	0.92	4
27.63	40.24	−20.04	−4.12	1.9	2	2.25	0.12	4
27.59	40.59	−21.74	−4.27	1.9	1.8	6.84	−0.46	4
27.42	39.78	−17.81	−4.94	1.4	1.4	−4.96	−3.62	4
27.3	40.38	−20.7	−5.41	1.8	1.8	3.23	0.19	4
27.27	39.58	−16.83	−5.53	1.9	2	−2.43	0.49	4
27.22	39.9	−18.38	−5.72	1.2	1.1	−0.48	−1.85	4
27.21	40.17	−19.68	−5.76	1.9	1.9	0.72	−2.33	4
26.91	40.03	−18.98	−6.94	1.9	1.9	0.04	−0.95	4
26.88	40.4	−20.77	−7.06	1.7	1.8	4.02	1.33	4
26.32	39.78	−17.72	−9.25	1.9	2	−0.78	0.38	4
26.22	39.73	−17.47	−9.64	1.9	1.9	−2.23	−0.22	4
26.19	39.61	−16.88	−9.76	1.9	1.9	−0.81	0.71	4
26.17	39.97	−18.62	−9.84	1.2	1.1	3.13	0.35	4
26.16	39.73	−17.46	−9.88	1.9	1.9	−1.63	1.31	4
26.08	39.5	−16.34	−10.19	2	2	−2.34	2.15	4
25.13	39.85	−17.91	−13.91	1.2	1.1	2.98	1.53	4
28.94	40.3	−20.36	1.02	2.86	3.32	6.13	1.85	4
28.92	39.93	−18.57	0.94	3.01	3.47	−5.04	−2.38	4
28.88	40.48	−21.23	0.78	1.5	1.67	4.01	8.14	4
28.09	39.92	−18.51	−2.31	0.3	0.3	−1.22	−1.84	4
27.91	40.09	−19.33	−3.02	0.3	0.3	−0.48	−1.58	4
27.91	39.72	−17.54	−3.02	0.3	0.3	−2.45	−1.19	4
27.84	40.39	−20.78	−3.29	1.8	1.83	5.87	0.51	4

Table 2. (continued)

Longitude, °E	Latitude, °N	v_{east}	v_{north}	σ_{east}	σ_{north}	m_{east}	m_{north}	Euler Vector[b]
27.82	40.4	−20.83	−3.37	0.9	1.06	2.13	1.39	4
27.76	40.06	−19.18	−3.61	0.75	0.9	−2.29	0.21	4
27.71	40.03	−19.03	−3.8	0.3	0.3	−1.33	−1.69	4
27.63	40.24	−20.04	−4.12	3	3.33	5.69	1.67	4
27.59	40.59	−21.74	−4.27	0.9	0.92	7.17	−0.06	4
27.42	39.78	−17.81	−4.94	1.05	1.35	−2.28	−1.69	4
27.3	40.38	−20.7	−5.41	2.1	2.42	1.01	0.12	4
27.27	39.58	−16.83	−5.53	1.05	1.21	−2.02	−0.86	4
27.22	39.9	−18.38	−5.72	0.6	0.61	−0.78	−3.05	4
26.91	40.03	−18.98	−6.94	3.15	3.34	1.39	−1.77	4
26.88	40.4	−20.77	−7.06	0.75	0.9	6.67	0.45	4
26.73	39.65	−17.13	−7.64	2.7	3.02	−3.31	0.93	4
26.53	39.58	−16.77	−8.43	0.9	1.05	−2.12	0.62	4
26.32	40.26	−20.04	−9.25	1.8	1.97	−0.94	−0.34	4
26.32	39.78	−17.72	−9.25	2.7	3.16	0.26	−1.51	4
26.19	39.61	−16.88	−9.76	1.22	1.08	−3.04	−0.36	4
26.17	39.97	−18.62	−9.84	0.45	0.46	1.59	0.12	4
26.16	39.73	−17.46	−9.88	3	3.32	−2.86	1.92	4
28.92	39.93	−18.57	0.95	1.66	1.63	−6	−2.13	4
27.91	39.72	−17.55	−3.03	0.79	0.7	−4.26	−0.51	4
27.82	40.4	−20.83	−3.39	0.86	0.83	1.7	2.55	4
27.76	40.06	−19.17	−3.59	1.48	1.5	−4.72	1.05	4
27.63	40.24	−20.07	−4.12	1.52	1.59	1.91	0.45	4
27.59	40.59	−21.73	−4.29	1.19	1.12	6.25	−0.51	4
27.42	39.78	−17.83	−4.92	1.04	1.04	−5.41	−3.49	4
27.3	40.38	−20.71	−5.41	1.33	1.36	2.82	0.62	4
27.27	39.58	−16.82	−5.53	1.53	1.58	−2.86	0.97	4
27.21	40.17	−19.69	−5.75	1.45	1.52	0.4	−1.98	4
27.22	39.9	−18.36	−5.73	0.79	0.76	−1.04	−1.28	4
26.91	40.03	−18.98	−6.94	1.5	1.53	−0.37	−0.61	4
26.88	40.4	−20.75	−7.06	1.28	1.37	3.83	1.87	4
26.53	39.58	−16.77	−8.41	3.82	3.99	−5.79	−1.74	4
26.32	39.78	−17.74	−9.26	1.48	1.6	−1.36	0.69	4
26.22	39.73	−17.45	−9.66	1.54	1.57	−2.87	0.16	4
26.19	39.61	−16.9	−9.76	1.44	1.47	−1.24	1.18	4
26.17	39.97	−18.64	−9.82	0.77	0.68	1.98	1	4
26.16	39.73	−17.47	−9.89	1.45	1.48	−2.26	1.74	4
26.08	39.5	−16.34	−10.18	1.55	1.58	−2.85	2.56	4
29.51	40.16	−19.67	3.25	2.2	2.1	−1.53	−3.73	4
29.15	40.46	−21.13	1.84	2	2	1.45	0.25	4
28.37	40.4	−20.84	−1.22	2.1	2	−0.19	−1.69	4
29.51	40.16	−19.67	3.25	1.06	1.21	−0.67	−2.43	4
29.29	40.48	−21.22	2.39	1.52	1.81	7.31	−0.56	4
29.15	40.46	−21.13	1.84	3.3	3.5	1.25	2.4	4
28.41	39.99	−18.86	−1.06	1.51	1.81	2.05	−3.1	4
28.37	40.4	−20.84	−1.22	1.2	1.36	1.83	−1.25	4
29.51	40.16	−19.69	3.27	1.81	1.7	−2.17	−4.19	4
29.15	40.46	−21.13	1.83	1.61	1.57	0.43	−0.04	4
28.37	40.4	−20.83	−1.2	1	0.93	−0.66	−0.74	4
28.78	40.17	−19.73	0.39	2	1.9	−0.22	−3.17	4*
28.78	40.17	−19.73	0.39	2.86	3.32	2.94	−3.29	4*
28.78	40.17	−19.72	0.39	1.54	1.55	−0.77	−3.24	4*
30.03	40.47	−21.14	5.29	1.2	1.1	4.32	−5.59	4*
29.93	40.42	−20.91	4.9	1.3	1.3	2.59	−6.29	4*
29.91	40.44	−21	4.82	1.4	1.5	3.39	−6.41	4*
29.68	40.36	−20.63	3.92	2.2	2	1.72	−1.91	4*
29.26	40.2	−19.87	2.27	2	1.9	−1.31	−4.05	4*
29.14	40.12	−19.48	1.8	1.3	1.2	−0.29	−2.28	4*
29.11	40.17	−19.73	1.69	2	1.9	−0.94	−2.56	4*
29.11	40.27	−20.21	1.69	2	1.9	−0.66	−1.67	4*
29.1	40.14	−19.58	1.65	1.4	1.3	−3.59	−4.92	4*
29.02	40.17	−19.73	1.33	2	1.9	−2.54	−1.31	4*
30.03	40.46	−21.09	5.29	0.3	0.31	5.64	−6.63	4*
30.02	40.44	−21	5.25	0.3	0.31	1.74	−7.09	4*
29.68	40.36	−20.63	3.92	0.46	0.6	1.05	−3.64	4*
29.26	40.2	−19.87	2.27	3.46	3.79	−1.62	−0.17	4*
29.14	40.12	−19.48	1.8	0.6	0.61	2.02	−1.78	4*
29.11	40.16	−19.68	1.69	2.86	3.18	3.02	−2.57	4*
29.11	40.27	−20.21	1.69	3.16	3.48	−0.15	−0.3	4*
29.1	40.14	−19.58	1.65	0.61	0.75	−3.17	−3.33	4*
29.02	40.17	−19.73	1.33	2.87	3.32	−4.51	−1.53	4*

Table 2. (continued)

Longitude, °E	Latitude, °N	v_{east}	v_{north}	σ_{east}	σ_{north}	m_{east}	m_{north}	Euler Vector[b]
30.03	40.47	−21.12	5.28	0.75	0.68	3.71	−5.81	4*
29.93	40.42	−20.93	4.9	0.85	0.83	2.15	−5.53	4*
29.91	40.44	−20.99	4.81	0.94	0.96	3.41	−5.78	4*
29.68	40.36	−20.64	3.92	0.94	0.78	0.24	−3.34	4*
29.26	40.2	−19.87	2.28	1.62	1.56	−2.06	−4.37	4*
29.14	40.12	−19.49	1.81	0.89	0.86	0.55	−0.25	4*
29.11	40.17	−19.7	1.69	1.55	1.55	−1.49	−2.64	4*
29.11	40.27	−20.21	1.67	1.54	1.52	−1.57	−2.03	4*
29.1	40.14	−19.56	1.65	0.97	0.96	−4.3	−5.1	4*
29.02	40.17	−19.74	1.35	1.54	1.54	−3.19	−1.55	4*

[a]Euler vector key is as follows: 1, Central Greece; 2, South Aegean; 3, Anatolia; 4, South Marmara.
[b]The asterisk indicates a station in an intraplate deforming zone.

data and the appropriateness of the merging approach applied here.

[11] In general, we have relied on the original references for estimates of uncertainties in site velocities. However, for the network analyzed by *Ayhan et al.* [2002] the stated uncertainties appear to be too small. Judging from results obtained from nearby nets studied by others that used similar survey procedures, time intervals, and repeat observations [*McClusky et al.*, 2000; *Meade et al.*, 2002], the uncertainties of *Ayhan et al.* [2002] are too small by about a factor of 2 to 5. In modeling microplate motions (see next section) we carry out inversions both including and excluding the *Ayhan et al.* [2002] data. Inversion results are insensitive to these differences in input, but misfits to the preferred model are notably larger for the *Ayhan et al.* [2002] data.

3. Aegean Velocity Field and Four-Microplate Model

[12] Several aspects of the Aegean velocity field are particularly noteworthy. The most striking feature of Figure 2 is the much smaller magnitude of the velocities north of the North Aegean Trough and north of latitude ~39.7°N in central Greece. Where sites are sufficiently densely spaced across this zone the GPS velocity gradients are high, showing that 60–70% of Eurasia-South Aegean relative motion occurs here. Figure 2 also reveals three key features of the motions that are crucial to understanding where current deformation occurs. (1) Anatolia is moving WSW at 15 to 25 mm/yr relative to Eurasia. (2) The South Aegean (and much of the Peloponnese) move SSW at ~30 mm/yr. (3) Central Greece is rotating clockwise, with GPS site motions relative to Eurasia increasing from 5 mm/yr in NW Greece to 20 mm/yr at Volos (V, Figure 2) and 30 mm/yr at Evia (E). These features of the GPS velocity field reflect the motions of stable blocks in central Greece, Anatolia, and the South Aegean.

[13] Previous GPS studies have demonstrated the rigid rotation of core regions in central Greece [*Le Pichon et al.*, 1995], central Anatolia and the southern Aegean [*McClusky et al.*, 2000], and the Marmara region [*Meade et al.*, 2002; *Le Pichon et al.*, 2003; *Flerit et al.*, 2003]. Here we build on these results using the complete velocity field in Figure 2 to identify deforming regions, rigid elements, and potential microplate boundaries. We used an iterative approach, tentatively defining microplate boundaries, determining best fit rigid rotations, examining misfit patterns, and revising the microplate boundaries to achieve a better match between model and data. Following *Le Pichon et al.* [1995, 2003] and *McClusky et al.* [2000] we initially specified four microplates (central Greece, Anatolia, South Aegean, South Marmara) and used the velocity field in Figure 2 as a guide to locate trial boundaries. The predicted velocities for the best fit four-microplate model, and their residuals, are plotted in Figure 3. Euler vector model parameters and misfit statistics are listed in Table 4.

[14] We first assessed the rigidity of each microplate by examining the match between observed and model predicted velocities at each GPS site. Later we use the misfit residual vectors in Figure 3 to quantitatively estimate intraplate strain rates (see Table 5 and discussion below). The misfits to the preferred four-microplate model cited below exclude the *Ayhan et al.* [2002] data because of

Table 3. Helmert Transformation Parameters in a Cartesian Coordinate System, RMS Misfits, and Uncertainty Estimates[a]

Helmert Transformation Parameters									
T_x, m/yr	T_y, m/yr	T_z, m/yr	S ($\times 10^{-9}$)	W_x ($\times 10^{-9}$), rad/yr	W_y ($\times 10^{-9}$), rad/yr	W_z ($\times 10^{-9}$), rad/yr	RMS Misfit	Number of Mutual Sites	Source
0.0141	0.0130	−0.0117	−1.11	3.66	−2.01	1.45	2.21	6	*Clarke et al.*
± 0.0263	± 0.0414	± 0.0386	± 3.92	± 5.45	± 5.90	± 5.48			[1998]
−0.0410	0.0127	−0.0017	4.32	5.85	3.20	−4.49	1.71	10	*Cocard et al.*
± 0.0209	± 0.0197	± 0.0192	± 1.64	± 1.91	± 3.99	± 3.23			[1999]
−0.0131	−0.0147	0.0074	1.49	−1.86	1.72	0.64	1.13	61	*Ayhan et al.*
± 0.0067	± 0.0092	± 0.0095	± 0.75	± 1.31	± 1.62	± 1.05			[2002]
−0.0016	−0.0010	−0.0101	1.25	1.12	−0.80	0.48	0.48	67	*Meade et al.*
± 0.0080	± 0.0098	± 0.0119	± 0.81	± 1.51	± 2.00	± 1.07			[2002]

[a]Parameters are computed by solving $\mathbf{dV} = \mathbf{T} + S\mathbf{r} - \mathbf{W} \times \mathbf{r}$, where $\mathbf{r}$ denotes station location, $\mathbf{dV}$ is the difference with the reference velocity field [*McClusky et al.*, 2000], $\mathbf{T}$ (T_x, T_y, T_z) is the translation vector, S is a scaling factor, $\mathbf{W}$ (W_x, W_y, W_z) is the rotation vector.

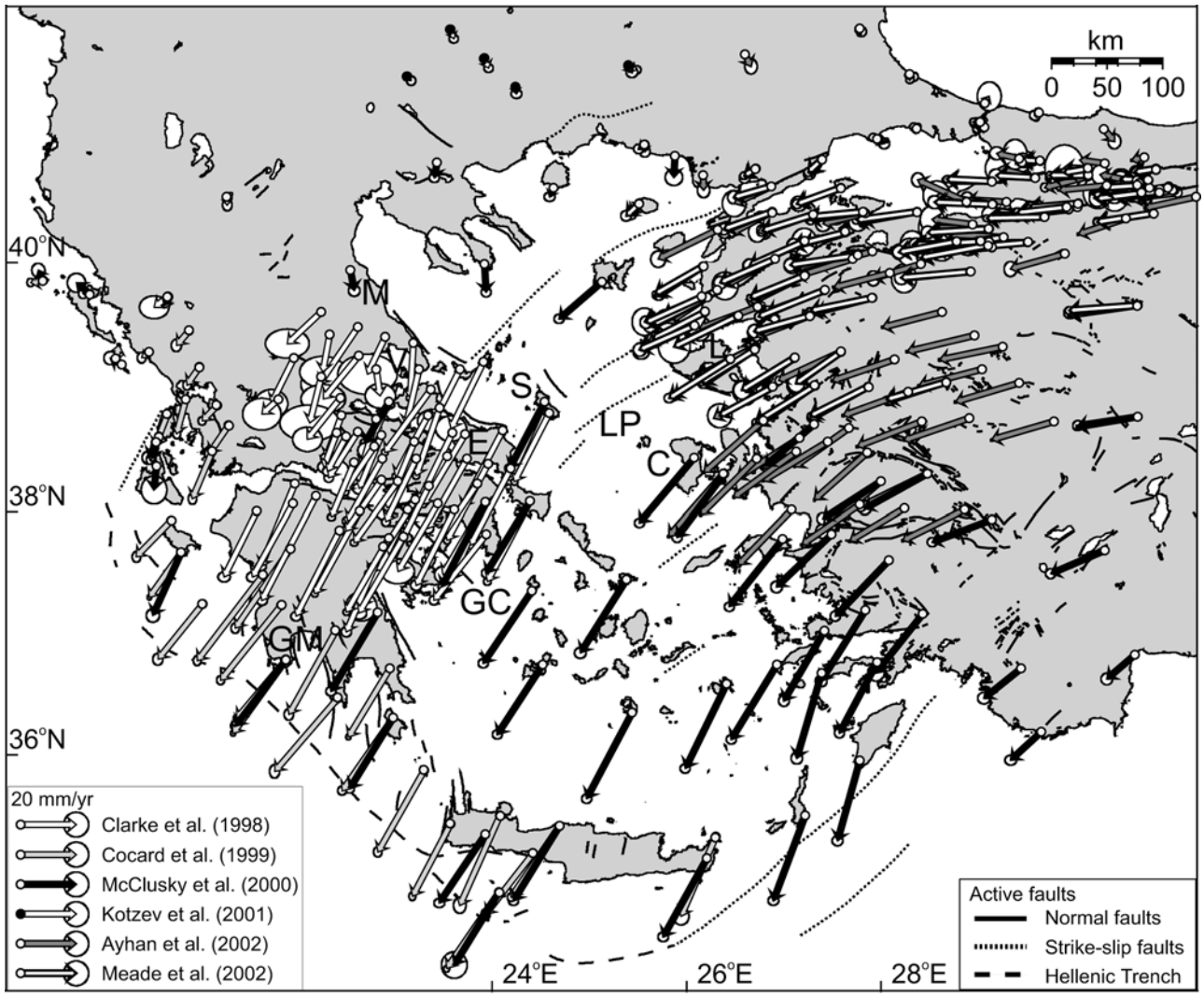

Figure 2. Observed GPS velocity field relative to stable Eurasia (to north of map area). One standard deviation error ellipses are shown for reference. Vectors are color coded to indicate the data source, as shown in the legend. Active faults are shown as in Figure 1. Geographic locations mentioned in the text include the following: C, Chios; E, Evia; GC, Gulf of Corinth; GM, Gulf of Messinia; L, Lesbos; LP, Lesbos-Psara Trough; M, Magnesia; S, Skyros; V, Volos. See color version of this figure in the HTML.

underestimation of velocity uncertainties discussed above. However, we do show misfit statistics for this network separately in Table 4. As expected they are 2 to 5 times larger than corresponding misfit values for other network data.

[15] Normalized misfits given in Table 4 are shown in two ways. MF_1 includes all the GPS vectors on an individual microplate and MF_2 deletes those vectors we judge are contaminated by internal deformation (see below). The MF_1 values average 2.6 and range from 2.0 to 3.7. The MF_2 values range from 1.7 to 2.1, which correspond to average misfit of GPS velocities ranging from about 2 to 5 mm/yr.

[16] Once the effects of the intraplate deforming zones have been taken into account the match between model and data is quite good, generally better than the typical fit between GPS data and coseismic fault models [e.g., *Hudnut et al.*, 1996; *Feigl et al.*, 2002]. Some of the residual misfits are likely due to elastic strain accumulation effects, which will be significant within several coseismc fault depths of the microplate boundaries [e.g., see *Thatcher*, 1995, Figure 4]. Within 15 km of the North Anatolian fault in the Sea of Marmara, *Le Pichon et al.* [2003] and *Flerit et al.* [2003] have shown that such effects are important and we do not use these site velocities to determine Euler vectors or assess misfit. As we show in Appendix A, at greater distances from this fault and near other microplate boundaries, strain accumulation corrections are small, do not influence our results, and are too uncertain to estimate reliably.

[17] The GPS velocities define several extensional zones apparently not directly related to the motions of the 4 identified microplates. This is best seen by examining residual GPS site velocities shown in Figure 3. Systematic patterns of residual velocities larger than about 5 mm/yr are judged to represent significant intraplate deformation. In each case this judgment includes assessing the uncertainties in (1) Helmert transformation adjustments (Table 3), (2) GPS data (Table 2), and (3) model plate motion vectors at each site. Uniform strain rates have been determined within

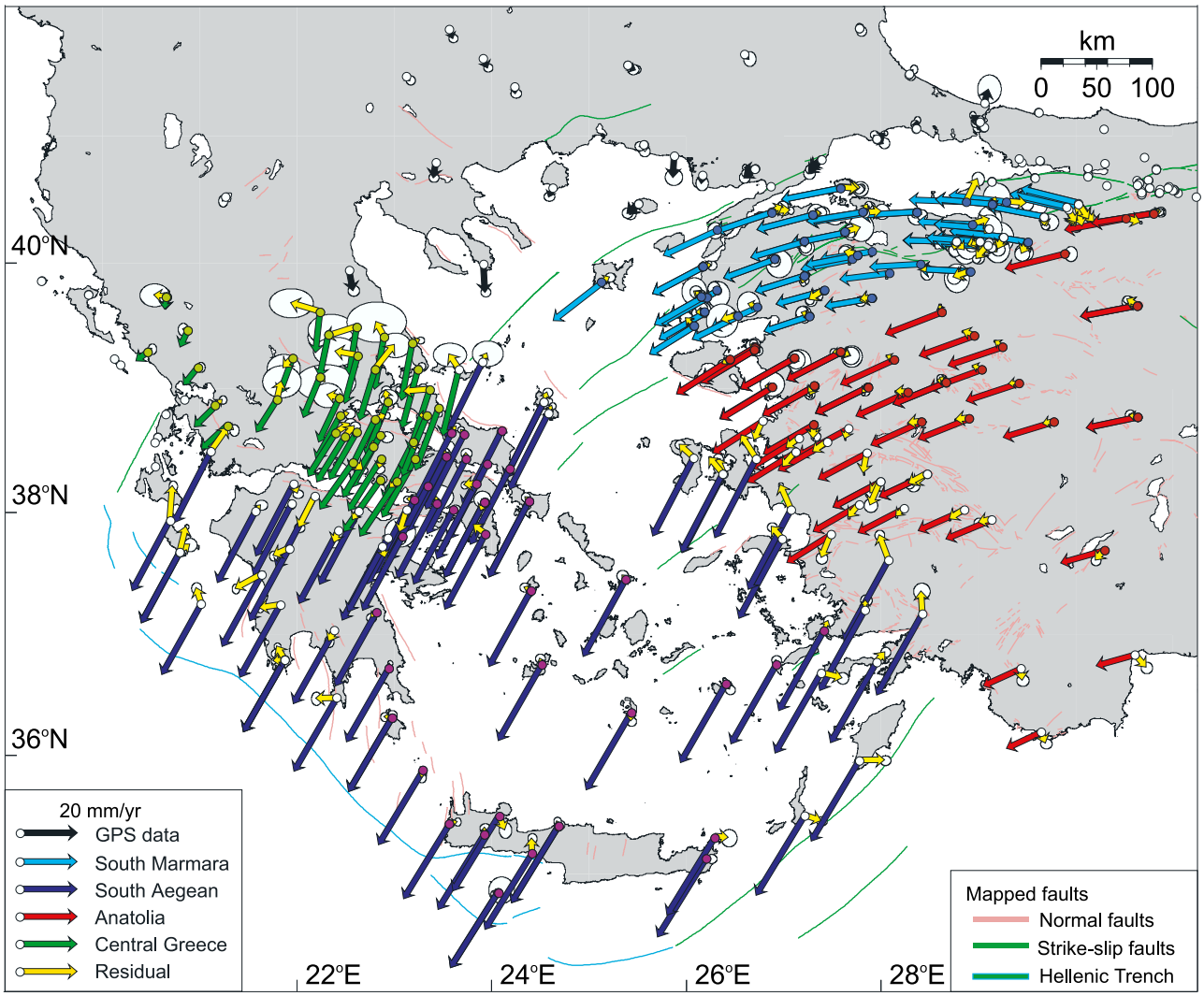

Figure 3. Predicted GPS site velocities relative to Eurasia (red, Anatolian plate; blue, South Aegean; green, Central Greece; cyan, South Marmara) and residuals (yellow) for the four-microplate model described in the text. Sites indicated by colored dots (red, Anatolia; purple, South Aegean; green, Central Greece) are assumed to be located on stable microplate interiors. One standard deviation error ellipses permit comparison of residuals with velocity uncertainties. Observed GPS site velocities on the Eurasian plate are shown in black.

each of these zones, and results are listed in Table 5 and plotted in Figure 4. In each of the identified internally deforming zones the orientation of the extensional strain axis generally agrees with the azimuths of slip vectors from earthquake fault plane solutions shown in Figure 1.

[18] In Bulgaria and northern Greece, south oriented velocities of 5–10 mm/yr relative to stable Eurasia cause ~N-S extension in at least two zones. Movements do not seem to be laterally continuous but station coverage is too sparse to define deforming zones well. The extensional principal strain rate averaged over this large region (see Figure 3) is 26 ± 9 nanostrain/year (nstrain/year) oriented N16°E, generally parallel to the T axes of normal fault earthquakes in this region (see Figure 1). Significant extension in southern Bulgaria was previously noted by *Kotzev et al.* [2001].

[19] Systematic patterns of residuals within several subregions of the South Aegean microplate suggest localized extension. In the southern and western Peloponnese these residuals suggest ~5 mm/yr of EW extension across mapped normal faults near the Gulf of Messinia (GM) and perhaps in adjacent regions. The extensional principal strain is oriented EW, ~perpendicular to the active normal faults of the region [*Lyon-Caen et al.*, 1988; *Armijo et al.*, 1992]. The average extension rate is 46 ± 20 nstrain/year. In the SE Aegean as much as 5–10 mm/yr of E-W extension may be occurring. The principal extensional strain rate is 47 ± 20 nstrain/year and is oriented N115°E, in close agreement with the N103°E oriented Plio-Pleistocene extension described in the tectonostratigraphical study of *ten Veen and Kleinspehn* [2002]. Deformation in these regions was previously suggested by *McClusky et al.* [2000].

Table 4. Microplate Euler Vectors Relative to Eurasia[a]

Region	Euler Vectors			MF1	MF2	MF3
	Latitude, °N	Longitude, °E	Rotation Rate, °/Myr			
Central Greece[b]	39.78 ± 0.02	19.99 ± 0.06	4.34 ± 0.10	2.3	2.1	2.2
South Aegean[b]	−45.91 ± 0.05	161.77 ± 3.61	0.52 ± 0.03	3.7	1.9	2.0
Anatolia[c]	−30.7 ± 0.8	32.6 ± 0.4	1.2 ± 0.1	2.1	1.7	1.8
				10.4[d]	8.6[d]	8.1[d]
South Marmara[e]	36.10	28.68	2.50	2.4	2.0	1.7
				6.0[d]	4.9[d]	3.2[d]

[a]Rotation is clockwise positive. To compare model predicted velocities with GPS velocity data we compute the normalized root-mean-square (NRMS) misfit function MF = $\sqrt{\frac{1}{N-f}\sum_{i=1}^{N}\frac{(v_i-p_i)^2}{\sigma_i^2}}$, where N is the number of velocity vectors, $f = 3$ is the number of degrees of freedom (Euler vector parameters), v_i is the GPS velocity vector at the ith site, p_i is the predicted motion at the ith site, σ_i is the standard deviation of v_i. MF1 is the NRMS misfit of the microplate model with all GPS vectors on the individual microplate (color coded lines in Figure 3); MF2 is the NRMS misfit with those GPS vectors that are located on the stable microplate interiors (color coded dots in Figure 3); MF3 is the NRMS misfit for stations on the stable microplate interiors after adjusting for elastic loading on the block boundaries and faults identified in Appendix A (with a locking depth of 10 km).

[b]The Euler vectors for the South Aegean and Central Greece are computed with the GPS vectors on the stable microplate interiors (color coded dots in Figure 3).

[c]The Euler vector for Anatolia is taken from *McClusky et al.* [2000].

[d]MF1, MF2, and MF3 values for *Ayhan et al.* [2002] data only.

[e]The Euler vector for South Marmara is taken from *Le Pichon et al.* [2003].

[20] GPS residuals SE of the Sea of Marmara suggest ~4 mm/yr of NNE oriented extension within the South Marmara block (see also Figure 6b and discussion below). The average extensional principal strain rate is 50 ± 9 nstrain/year oriented N18°E, generally parallel to the T axes of several normal fault earthquakes in the region. *Flerit et al.* [2003] previously noted extensional strains in this region.

[21] Finally, residuals in SW Anatolia suggest an E-W oriented region with ~5 mm/yr of extension across it. The extensional principal strain rate is 47 ± 8 nstrain/year oriented N27°E, nearly perpendicular to the major normal faults of the region.

[22] The microplate boundaries and the spatial distribution of Aegean deformation inferred from the GPS results and supporting data are shown in Figure 5. The observed deformation results both from relative motions of the four stable blocks and localized straining internal to the blocks, producing a pattern of both continuous and discontinuous deforming zones. The block boundaries and relative motions across them are independently constrained where GPS station density is high, for example near the Gulf of Corinth and the west coast of Anatolia. In other locations, like NW Greece, NW Anatolia, and the north central Aegean, the boundaries are uncertain and relative motions shown in Figure 5 are extrapolations based on the rigid microplate model. In such regions the magnitude and direction of relative motion are well constrained by the model, but the sense of slip across the boundary depends upon its precise orientation. The orientation and location are often not well known, although earthquake distributions and fault plane solutions are useful as rough guides.

Table 5. Uniform Strain Rates With 1 Standard Deviation Uncertainties for Different Microplates and Internally Deforming Zones

Region	Id[a]	Model	No.[b]	Axis 1[c]		Axis 2[c]		MF Before[e]	MF After[e]
				Nanostrain/Year[d]	Azimuth, deg	Nanostrain/Year[d]	Azimuth, deg		
Central Greece	1	all stations	39	E 26 ± 14	−21	**C 23 ± 11**	−111	2.3	2.3
Central Greece	**2**	rigid	38	E 24 ± 14	−23	**C 24 ± 12**	−113	2.1	2.1
South Aegean	3	all stations	80	E 4 ± 2	95	E 2 ± 2	5	3.7	3.7
South Aegean	**4**	rigid	40	E 2 ± 4	111	C 4 ± 4	−159	1.9	1.9
South Aegean	**5**	Peloponnese	10	**E 46 ± 20**	90	C 30 ± 21	180	3.5	2.3
South Aegean	**6**	Southeast Aegean Sea	10	**E 47 ± 20**	115	E 13 ± 19	25	2.8	1.7
Anatolia	7	all stations	70	**E 18 ± 2**	16	**E 5 ± 2**	105	2.1; 10.4[f]	1.8; 6.8[f]
Anatolia	**8**	rigid	52	**E 13 ± 4**	37	C 7 ± 4	−53	1.7; 8.6[f]	1.4; 5.8[f]
Anatolia	**9**	deformation zone	25	**E 47 ± 8**	27	C 15 ± 8	−63	9.8	4.0
South Marmara	10	all stations	116	**E 37 ± 8**	21	C 11 ± 8	−69	1.8; 3.8[f]	1.3; 2.9[f]
South Marmara	**11**	rigid	41	E 12 ± 14	35	C 24 ± 15	−55	1.7; 3.2[f]	1.0; 1.6[f]
South Marmara	**12**	deformation zone	115	**E 50 ± 9**	18	C 3 ± 9	−72	4.3	3.1
Northwest Greece	**13**	all stations	15	**E 26 ± 9**	16	C 9 ± 8	−74	2.9	1.5
Northeast Greece	**14**	all stations	13	E 14 ± 13	54	C 18 ± 14	144	2.1	1.7

[a]Id numbers in bold indicate those regions for which the principal strain rates are plotted in Figure 4.

[b]Number of stations that contribute to the strain estimate.

[c]Principal strain rates, where C and E indicate contraction and extension, respectively.

[d]Principal strain rate values in bold are significant at the level of twice the standard deviation.

[e]NRMS misfit values computed as in Table 3: "MF before" is the misfit between the GPS velocity data and the rigid block model velocity field adjusted for elastic loading on the North Anatolian fault with a locking depth of 10 km (see also Figure A1 and Table A1). "MF after" is the misfit between the GPS velocity data and the combined model of rigid block motion, elastic loading on the North Anatolian fault zone and regionally uniform strain and rotation rates.

[f]MF values for *Ayhan et al.* [2002] data only.

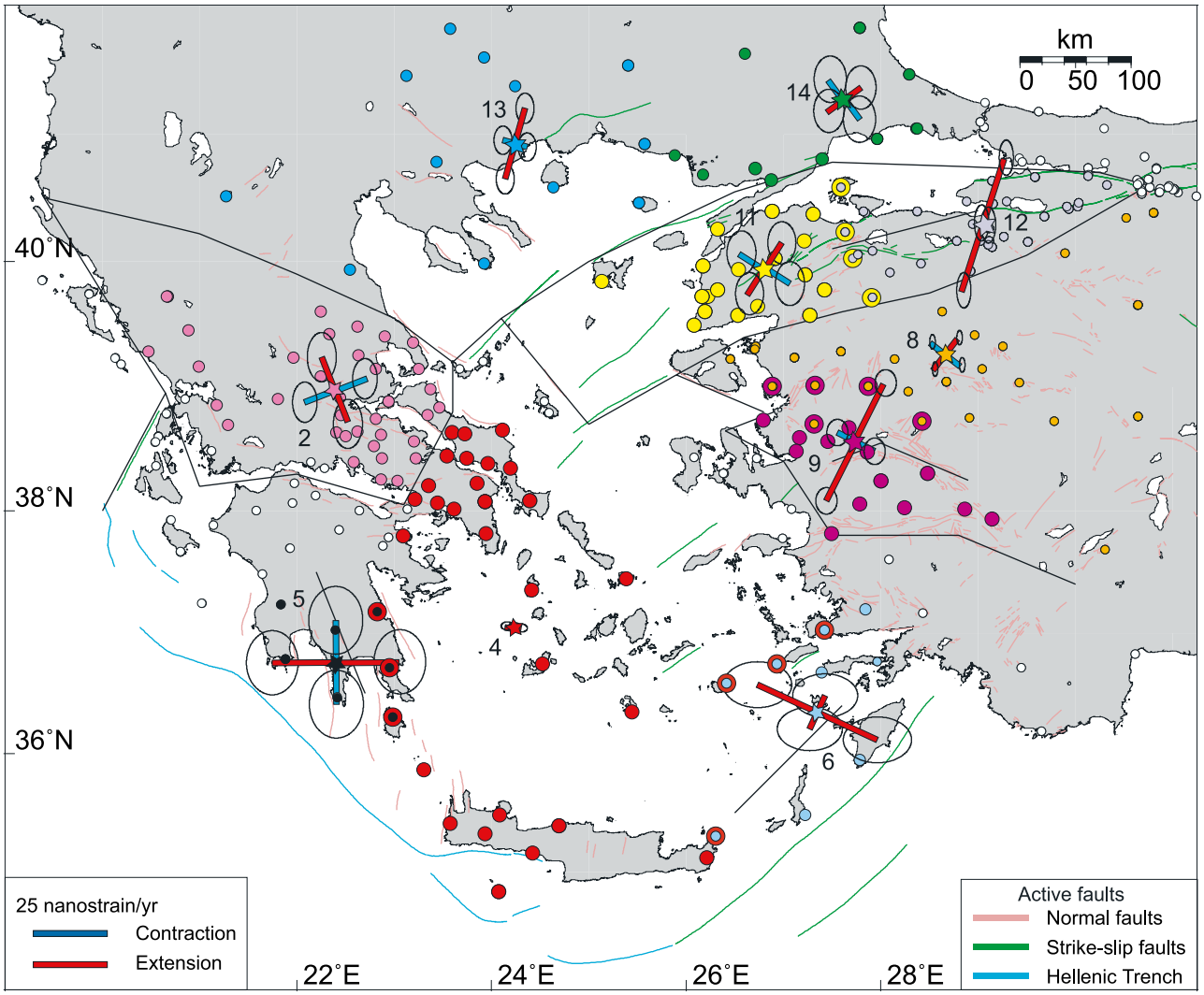

Figure 4. Principal strain rates within identified internally deforming zones (see Figure 5) and within microplate interiors (excluding internally deforming zones). Dots are GPS stations, color coded to indicate the sites used in each independent strain rate estimation, which is centered at a star symbol of the same color. One standard deviation error ellipses are shown at the tips of each principal strain rate axis. All strain rate values are listed in Table 5.

[23] Deformation rates in the microplate interiors are small or negligible except within the identified internal extension zones shown in Figure 5. As Table 5 shows, strain rate determinations are typically uncertain to ±10–20 nstrain/year, corresponding to velocity uncertainties of 1 to 2 mm/yr over distances of 100 km. Except within the Anatolia microplate, no strain rates exceed zero by more than two standard deviations (see Table 5). Within Anatolia, there are over 50 very precisely determined GPS velocities, and we find a small but resolvable extension rate of 13 ± 4 nstrain/year oriented N37°E, roughly perpendicular to regional normal faults and parallel to the T axes of earthquakes. These measurements are thus detecting strains related to the diffuse intraplate seismicity and active faults of central Anatolia. Better determinations of GPS velocities within other microplates might well resolve measurable strain rates of comparable magnitude. Note, however, that observed velocity gradients across the microplate boundaries are typically 20–100 times larger, about 10–20 mm/yr over distances of ~20 km, implying strain rates of ~500 to 1000 nstrain/year.

[24] The microplate motions have a number of direct consequences. Clockwise rotation of central Greece has two effects. First, this rotation and the SW translation of the Peloponnese and South Aegean cause the Gulf of Corinth to open by ~N-S extension. Gulf extension increases from ~5 mm/yr or less beyond its eastern edge to ~15 mm/yr in the central gulf and reaches as much as ~20 mm/yr farther NW. Second, rotation of central Greece relative to Eurasia produces from 5 to 20 mm/yr of relative motion, predominantly extension, at or near the northern boundary of this block from southern Albania to offshore Magnesia (M). However, because the GPS results show 5–10 mm/yr of south directed extension in Bulgaria and

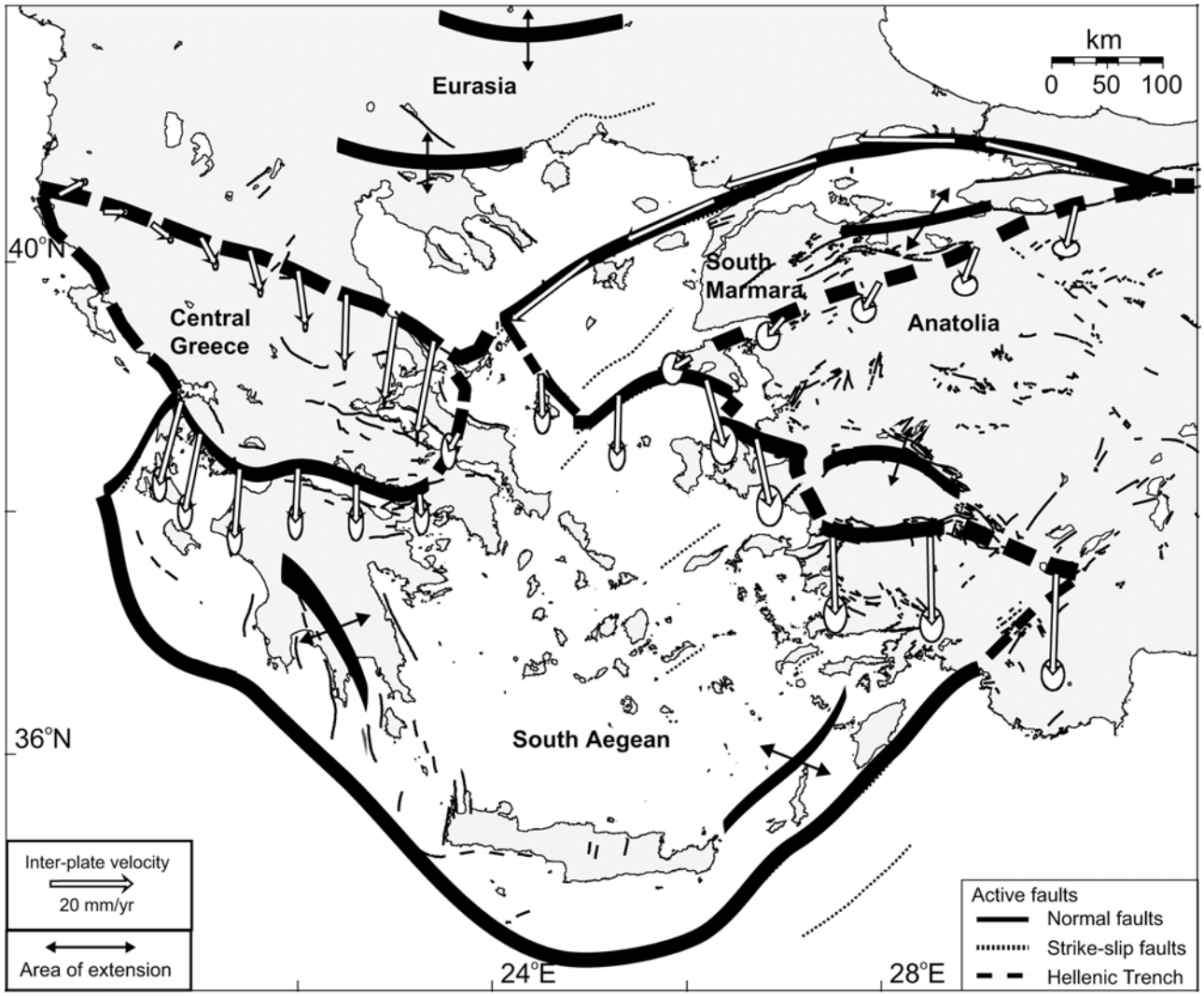

Figure 5. Schematic mapping of stable microplates and their approximate boundaries inferred from GPS results, active fault distribution, and earthquake fault plane solutions. Predicted relative motions across microplate boundaries are shown by arrows that indicate the motion of the south bounding block with respect to the north bounding block. Two standard deviation error ellipses are shown for reference. See color version of this figure in the HTML.

northern Greece with respect to stable Eurasia (Figure 2), the actual maximum extension across the Eurasia-central Greece boundary is likely to be only 10–15 mm/yr.

[25] The westward motion of South Marmara produces deformation on its northern and southern boundaries. Predicted South Marmara-Eurasia motion across the northern North Anatolian fault and the North Aegean Trough is 23 mm/yr of almost pure right-lateral strike-slip. The South Marmara/Anatolia relative motion decreases from 11 mm/yr of oblique extension SE of the Sea of Marmara to 5 mm/yr of strike-slip motion at the Aegean Sea coast. In the north central Aegean we locate the microplate boundary along the Skyros (S) Trough, then ENE along the Lesbos-Psara Trough (LP). Although the predicted motion is largely extensional at rates of 10–15 mm/yr, most of the fault plane solutions in this region are strike-slip (Figure 1). However, the location of the boundary is only poorly constrained, and some combination of left-lateral strike-slip on NNW oriented faults and extension on east trending normal faults may explain the predicted relative motion in this region. The 2001 $M = 6.4$ Skyros earthquake provides direct evidence for left-lateral strike-slip faulting near the Skyros Trough [*Karakostas et al.*, 2003]. Its focal mechanism is identified in Figure 1.

[26] Anatolia/South Aegean relative motion is predicted to be largely extensional. South of Lesbos (L) oblique extension is about 15 mm/yr. Farther ESE in SW Anatolia the microplate boundary is defined largely by GPS sites assigned to either the Anatolian or South Aegean blocks. Normal fault motions are consistent with the predicted relative motions, the fault distributions and the earthquake fault plane solutions. Larger GPS residuals near the inferred boundaries (see Figure 3) likely reflect complexities in the actual faulting and/or unmodeled effects of elastic strain accumulation across them. Some of the ~20 mm/yr of extension predicted across the southern EW fault segment

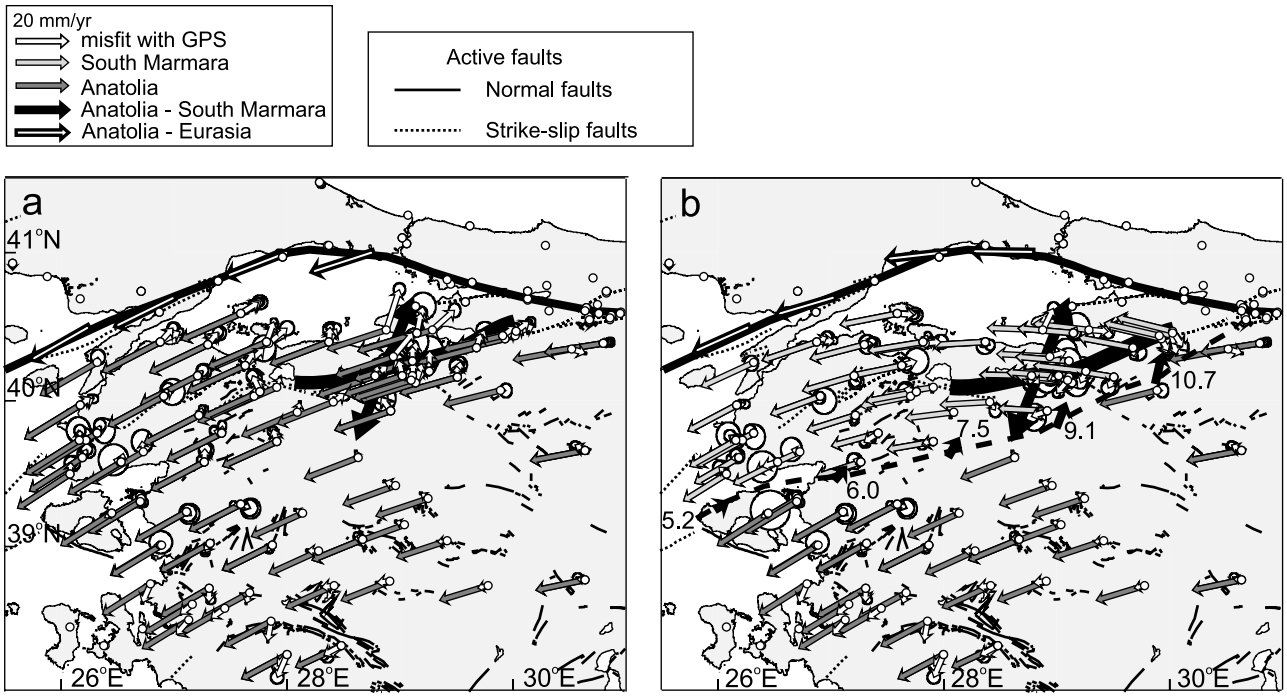

Figure 6. Predicted GPS site velocities relative to Eurasia in northwest Anatolia. One standard deviation error ellipses permit comparison of residuals with velocity uncertainties. (a) Predicted velocities for Anatolia Euler vector only. (b) Predicted velocities for South Marmara Euler vector of *Le Pichon et al.* [2003] and Anatolia Euler vector. Southern boundary of South Marmara block from *Le Pichon et al.* [2003] is shown by a dashed line with relative velocities between South Marmara block and Anatolia with rates in millimeters/year. See color version of this figure in the HTML.

may be accommodated across the isolated intraplate deformation zone inferred to lie immediately to the north of it.

4. South Marmara Block

[27] In accord with several recent studies [*Meade et al.*, 2002; *Le Pichon et al.*, 2003; *Flerit et al.*, 2003] our work supports the existence of an independent microplate in NW Anatolia bounded by the northern and southern branches of the North Anatolian fault. *Le Pichon et al.* [2003] used GPS data corrected for interseismic strain accumulation near the northern branch of the North Anatolian fault (NNAF) to determine a South Marmara/Eurasia Euler vector. They convincingly showed that the orientation of GPS vectors near the NNAF defined the small circle of an Euler pole distinct from the Anatolia/Eurasia pole and lying to the north of it. Such an Euler pole requires nearly pure strike-slip motion along a trend defined by on-land faults and by bathymetric lineations in the northern Sea of Marmara. *Le Pichon et al.* [2003] also suggested a partitioning between strike slip on the NNAF and extension on or near the southern branch of the fault [see also *Meade et al.*, 2002; *Flerit et al.*, 2003].

[28] There is thus considerable support for an independent microplate in the Marmara region. However, the GPS data cannot easily distinguish between this model and an Anatolia-only model with strike-slip faulting on the NNAF and intraplate extensional deformation localized south and southeast of the Sea of Marmara. Figure 6 shows the evidence for both viewpoints.

[29] Figure 6a is an enlargement of NW Anatolia and shows predicted velocities and residuals for a model that includes only the Anatolia plate. This model predicts oblique extension across the NNAF, and as mentioned above *Le Pichon et al.* [2003] have shown this is not consistent with GPS vectors near the fault (not shown in Figure 6a). North directed misfit vectors in Figure 6a south and east of the Sea of Marmara are also significant. These residuals could be explained by north-south extension on east striking intraplate faults located to the south of these sites within the Anatolia microplate. A modification to the Anatolia plate model in which pure strike-slip motion is enforced on the NNAF and necessary extension taken up on an intraplate zone south of the Sea of Marmara could account for all the main features of the GPS velocity field without requiring a South Marmara block.

[30] The inclusion of a South Marmara block (Figure 6b) successfully reproduces the GPS vectors near the NNAF, and the normalized RMS misfit of data within the block shown in Figure 6a has been reduced from 3.0 to 2.0 (see Table 4). There is also a significant improvement in the fit of data on the newly defined Anatolia plate (MF_2 decreases from 2.6 to 1.7). Application of an *F* test [*Stein and Gordon*, 1984] indicates the improved match to data resulting from inclusion of the South Marmara microplate is statistically significant.

[31] However, south directed residual vectors of 2 to 5 mm/yr are present south of the Sea of Marmara [see also *Le Pichon et al.*, 2003, Figure 9]. These residuals could be explained by intraplate extension within the South Marmara block. However, such extension would be in addition to the 8 to 11 mm/yr of oblique extensional motion that the model already requires at the southeastern boundary between the South Marmara and Anatolian microplates (arrows with numbers indicating rate in Figure 6b).

[32] On balance we favor the inclusion of a South Marmara block in NW Anatolia, but doubts remain. The somewhat smaller magnitude of residual vectors south and SE of the Sea of Marmara in Figure 6b relative to Figure 6a slightly favor the South Marmara model, but still requires internal deformation of the South Marmara block. Predicted motions near the Aegean coast are similar for both models, so the GPS data there cannot distinguish between them. An Anatolia-only model with pure strike-slip motion on the NNAF and necessary intraplate extension south of the Sea of Marmara remains a possibility.

5. Comparison With Previous Studies

[33] Figure 7 summarizes the kinematic patterns of deformation proposed in each of seven major studies that have notably advanced understanding of Aegean tectonics during the last 30 years. Comparison with Figures 5 or 7h shows that several key features of our GPS-based model have been suggested in this previous work, but others are surprising, and the overall pattern could not have been anticipated or mapped using either global plate tectonic models or pre-GPS indicators of Aegean deformation.

[34] *McKenzie* [1972, 1978] was the first to use plate tectonic principles, seismicity, fault plane solutions and active fault distributions to define the Aegean's major tectonic elements and suggest a plate-like model for the kinematics. The model (Figure 7a) has three rigid elements and also includes several zones of intraplate deformation in western Anatolia. Ironically, this model is perhaps closest to the one we favor, although McKenzie and others have subsequently found good reasons to repudiate specific features of this early "plate tectonic" model. In particular, the distribution of seismicity and active faulting is more widespread than was believed could be rationalized by McKenzie's model, and there was no evidence for strike-slip faulting in central Greece (see Figure 1), where his model postulates a transform fault connecting two zones of extension.

[35] *McKenzie and Jackson* [1983, 1986] were the first to suggest that clockwise rotation of crustal blocks in central Greece was required to explain the absence of strike-slip faulting and predominance of normal faulting observed there (see Figure 7b). They reasoned that the N-S orientation of earthquake slip vectors in central Greece could be reconciled with expected SSW motion relative to Eurasia if the normal faults and intervening blocks of crust in central Greece were rotating clockwise with respect to Eurasia. Our results define only one largely undeformed microplate in central Greece where *McKenzie and Jackson* [1983, 1986] predict several rotating "slats," but one expected effect of their predicted block rotation is nicely confirmed by the GPS data itself. The normal fault slip vector azimuths for Gulf of Corinth earthquakes clusters around 180°, and Figure 8 shows this agrees with the direction of relative motion between the central Greece and South Aegean microplates across the gulf (yellow line, 177°) determined solely from the GPS data analyzed here.

[36] *Taymaz et al.* [1991] noted the preponderance of strike-slip faulting in the northern Aegean and extension in central Greece and proposed a quantitative, nine-microplate, "broken slats" model (Figure 7c) to account for these features. With the great benefit of hindsight and more than a decade of GPS data we see this model as more complex than is necessary to explain the large-scale kinematics. However, our model can be viewed as a simpler, two-slat version of the Taymaz et al. model, with a central Greece slat rotating clockwise and a South Marmara slat showing counterclockwise rotation. It is also true that the partitioning of strike- and dip-slip motion remains an important observation that our four-microplate model is not particularly successful in explaining. Our model predicts predominantly extensional relative motion across the north central Aegean (see Figure 5), suggesting more normal faulting and dip-slip focal mechanisms between Skyros (S) and Lesbos (L) than are actually observed (Figure 1). If our model is essentially correct, the plate boundary in the north central Aegean may be more complex than is depicted in Figure 5.

[37] *Le Pichon et al.* [1995] presciently used early GPS measurements to quantify clockwise rotation of central Greece and westward increasing extension across the Gulf of Corinth. Although primarily focused on motions in central Greece, they suggested a two-block model of Aegean deformation with clockwise rotation of central Greece, counterclockwise rotation of the South Aegean and Anatolia, extension across the Gulf of Corinth, and a wide zone of distributed strike-slip deformation in the northern Aegean (Figure 7d). Their central Greece/Eurasia Euler vector (41°N, 18°E, 2.8°/Myr) is similar to ours (39.8°N, 20.0°E, 4.3°/Myr).

[38] *Armijo et al.* [1996] proposed a model emphasizing the necessary extensional end effects of right-lateral strike-slip fault termination in the NW Aegean and central Greece (Figure 7e). They suggested that present day extension is localized in the northern Aegean and central Greece near the ends and at offsets across the northern and southern branches of the North Anatolian fault. They proposed that lower rates of extension occur across several discrete arcuate zones in the central Aegean and SW Anatolia.

[39] *McClusky et al.* [2000] carried out a careful analysis and synthesis of a large set of high quality GPS data from western Greece to the South Aegean and western Turkey (green vectors in our Figure 2) and used their results to define rigid blocks in central Anatolia and the southern Aegean. In particular, they were the first to identify the South Aegean microplate and quantify its motion from the eastern Aegean to the SW Peloponnese. Our Euler vectors for Anatolia and the South Aegean microplates are very similar to theirs. *McClusky et al.*'s [2000] network contains few sites in mainland Greece and they did not consider its motion relative to the rest of the Aegean. However, they did suggest that much of the Aegean region is deforming by distributed extension that is widespread in Greece and within their study area in the northern Aegean Sea and

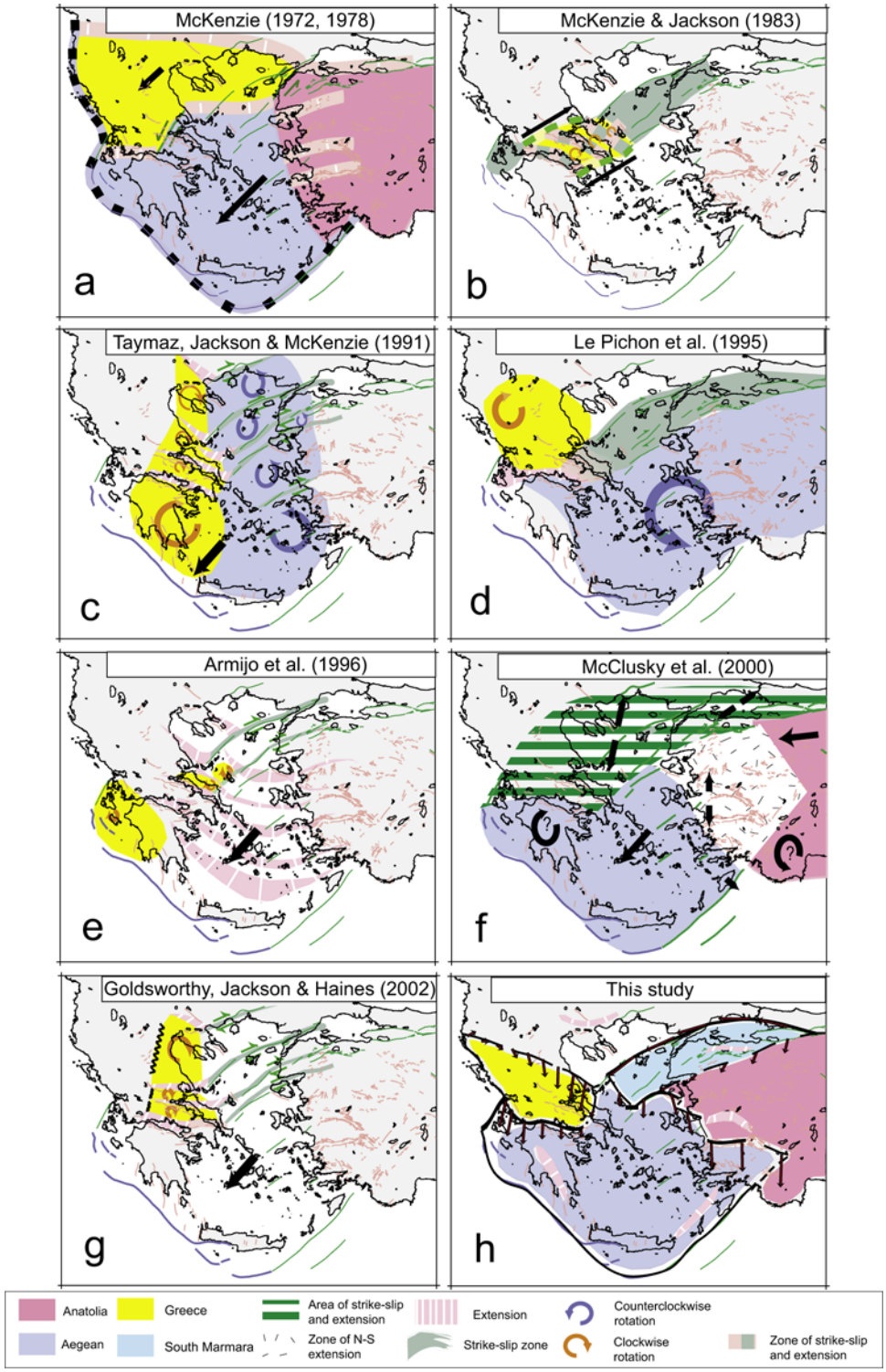

Figure 7. Kinematic models of Aegean tectonics (a–g) proposed in previous studies, compared with (h) model proposed here (from Figure 5).

western Anatolia (Figure 7f). Our results suggest most of this region is rigid, attached to the central Greece, Eurasian, South Aegean, South Marmara or Anatolian plates. A later short review by *Reilinger and McClusky* [2001] suggests greater rigidity in west and NW Anatolia, but does not assess it quantitatively or compare it with the more detailed treatment given by *McClusky et al.* [2000].

[40] *Goldsworthy et al.* [2002] use tectonic geomorphology integrated with seismic, geologic and GPS data to support a model for central and northern Greece that

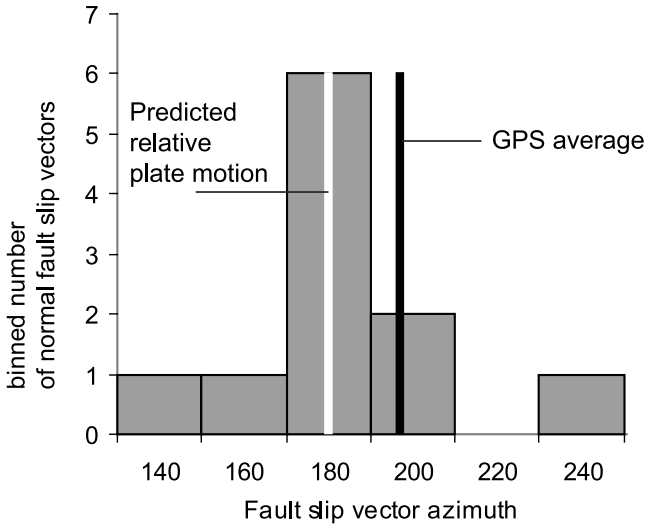

Figure 8. Histogram showing distribution of normal fault slip vector azimuths for Gulf of Corinth earthquakes. Average azimuth of local GPS velocity vector relative to Eurasia is shown (200°), along with observed direction of relative motion between central Greece and South Aegean microplates at the Gulf of Corinth (177°). Peak in the fault slip azimuth histogram disagrees with GPS vector azimuth but corresponds to direction of relative motion between central Greece and the Peloponnese computed here. See color version of this figure in the HTML.

includes three clockwise-rotating blocks with localized extension between them (Figure 7g). They further observe that extension in the Gulf of Corinth decreases to the east, while extension in the Gulf of Evia and grabens in Thessaly and Greek Macedonia decreases to the west. Block rigidity then requires Corinth opening be balanced by the summed extension across Evia, Locris and Thessaly. *Goldsworthy et al.* [2002] caution that their model is semiquantitative and should not be viewed too literally. Although GPS nets in northern Greece are sparse (see Figure 2) the available data do not support this three-block model. Bulgaria, Thrace and Greek Macedonia are moving ~south at 5–10 mm/yr with no evidence for the comparable strike-slip motion on the Kavali-Xanthi fault system (the northernmost block boundary) the model requires. Our model (Figure 5) requires all relative motion between central and northern Greece to occur across the North Aegean Trough while *Goldsworthy et al.* [2002] make it some unspecified fraction of the motion across their three northern block boundaries. They define a block boundary across central Evia that extends west into central Greece, while we see no evidence for relative motion across this zone. The Gulf of Corinth is a major block boundary in both models. In summary, the Goldsworthy et al. model specifies three rotating blocks in central and northern Greece while ours requires a single central Greece microplate and a zone of internal deformation in northern Greece.

[41] We have proposed a quantitative four-microplate model to explain first-order features of present day deformation of the entire Aegean region. In retrospect, it is surprising to us that such a simple model explains the GPS data as well as it does. However, our analysis also suggests the existence of isolated zones of deformation within the nominally rigid microplates and an indication of low rate internal straining within the Anatolia microplate. Comparable deformation may occur in zones lying outside current GPS networks, particularly in the NW Peloponnese and adjacent Ionian Sea and near the west coast of Anatolia. It is also possible that the apparently isolated zones are the boundaries of even smaller microplates. If so, the current GPS coverage is too sparse to identify their boundaries or determine their rigid motions. Furthermore, it is also important to note that the distribution of seismicity, active faults, and related geomorphic landforms indicate significant tectonic deformation that is occurring at or just below current GPS detection thresholds.

6. Global Plate Tectonics and Continental Tectonics

[42] Our results suggest that present-day continental tectonics, at least in the Aegean, is similar to global plate tectonics and follows the same kinematic rules. This view is not new and has had strong adherents since the early days of the development of plate tectonics. However, it has been and remains a contentious interpretation of continental tectonics. Several significant differences between deformation of oceanic and continental lithosphere, which we discuss below, have made this interpretation controversial. However, at least equally important is that the data and methods used to demonstrate plate kinematics so successfully in the oceans and on a global scale are of limited use on the continents. Indeed they may be misleading. In what follows we discuss each of these methods, contrasting their utility within ocean basins and on the continents with particular reference to the Aegean.

6.1. Identification of Plate Boundaries: Seismicity and Topography

[43] The distribution of earthquake epicenters in oceanic regions provided some of the most convincing evidence for the existence of plates [*Barazangi and Dorman*, 1969], and oceanic bathymetry maps showed that plate boundary seismicity coincided with the subsea topography of mid-ocean ridges, transform faults and trenches [*Morgan*, 1968]. On the continents, the wide distribution of extreme topography and seismicity in active regions has been logically cited as demonstrating the existence of broad regions of distributed deformation and evidence for a fundamental difference between the kinematics of global tectonics and continental deformation. As qualitative distinctions these observations usefully contrast continents and oceans, but they are of limited value in quantifying the kinematics of continental deformation.

[44] For example, Figure 9 shows that Aegean seismicity is generally not well correlated with the microplate boundaries identified from our GPS analysis. There is a general correspondence between the boundaries and concentrations of seismicity in several regions, for example along the North Aegean Trough, in the Gulf of Corinth, and near the Hellenic Trench. However, seismicity trends are present in many other regions, and the microplate boundaries defined by the GPS data cannot be located using seismicity alone.

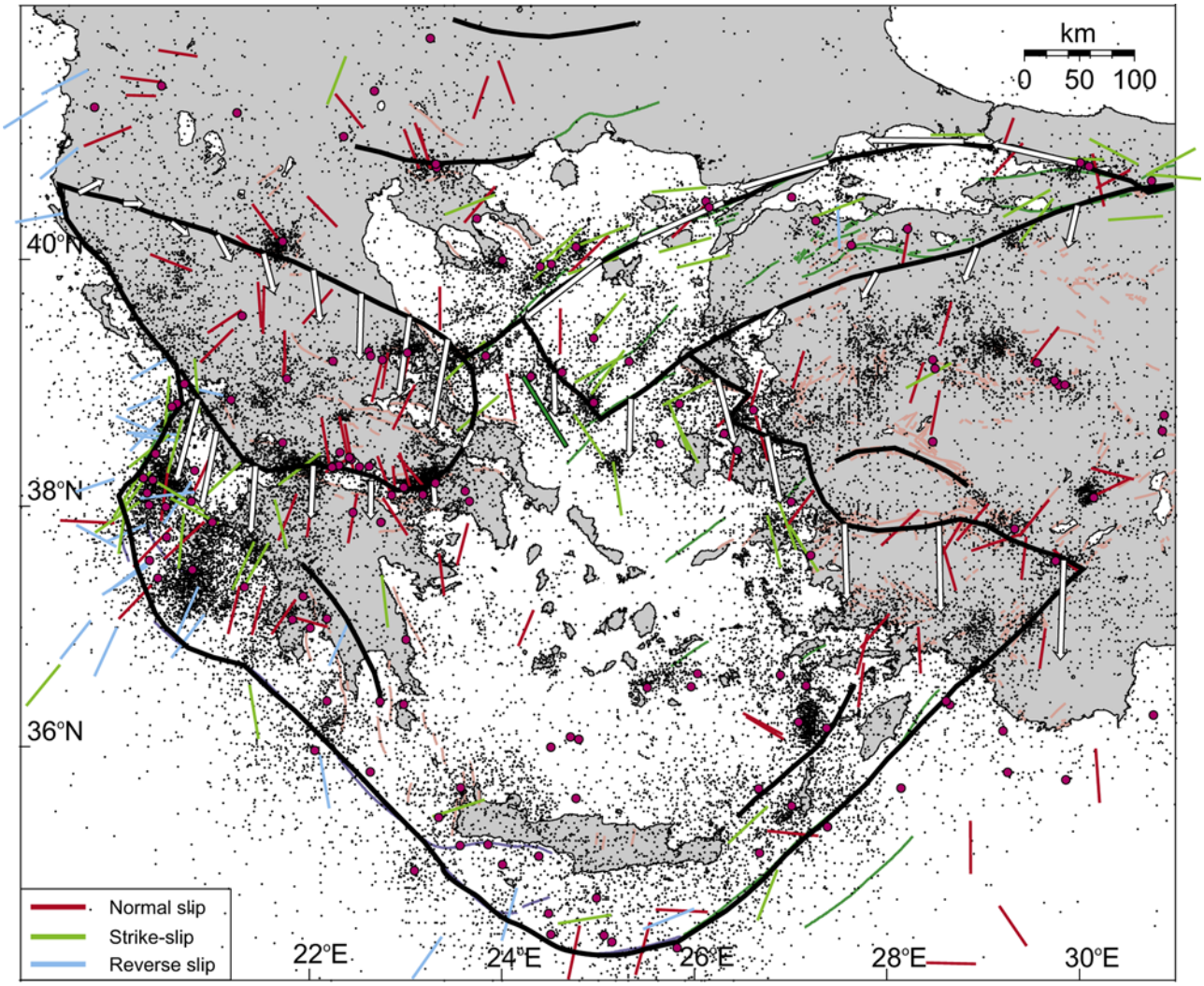

Figure 9. Microplate boundaries determined in this study, with large (M > 6) earthquakes during 1900–2000 (purple dots) from *Engdahl and Villasenor* [2002], smaller earthquakes from Greek and Turkish catalogs (small open circles), and earthquake slip vectors from fault plane solutions given in Figure 1. For each focal mechanism two slip vectors are possible. We have chosen the right-lateral vector for strike-slip faults. Normal and reverse slip vectors are consistent with the orientation and dip direction of nearby mapped faults. The 2001 M = 6.4 Skyros earthquake, discussed in section 3 (at approximately 24.5°E, 39°N) is indicated in a different shade of green.

Evidently the heterogeneity of continental lithosphere is sufficient to generate myriad zones of weakness where minor seismicity is distributed while most deformation is localized on a few of the weakest faults.

[45] Tectonic topography may also be a poor guide to large-scale present day kinematics. Relief due to extensional deformation is clearly evident throughout the Aegean both as subaerial and subsea basins and as uplifted footwall blocks of normal faults [e.g., *Jackson*, 1994]. However, impressive topography can be generated in a few million years by very modest slip rates on inclined faults. For example, normal faults slipping at rates less than a few mm/yr would be difficult to detect with current GPS coverage yet would generate a kilometer or more of Quaternary vertical offset. In general, fault topography can be generated quickly, in a few million years or less. However, because erosion rates in deactivated regions are much lower, typically 10–100 m/Myr [e.g., *Matmon et al.*, 2002], tectonic topography can persist for many millions of years, and only detailed geomorphic studies can distinguish currently active regions from those of low activity or dormancy. There is some evidence that several major Greek normal faults have been active for only the past million years or so [*Armijo et al.*, 1996; *Jackson*, 1999; *Goldsworthy et al.*, 2002]. Therefore, if faults are typically activated and deactivated on ~Ma timescales, and low slip rate faults generate significant relief, tectonic topography will be

much more diffusely distributed than is present day deformation.

6.2. Quantification of Plate Kinematics

[46] The transform fault orientations, dated magnetic anomalies, and earthquake slip vectors so effectively applied to determine global plate motions [e.g., *Demets et al.*, 1990] are not generally useful for quantifying continental microplate tectonics. There are of course no magnetic stripes on the continents. Continental transforms only occasionally and locally follow circular arcs defined by Euler poles, and slip vectors often do not show the relative motions across microplate boundaries. For example, only parts of the central North Anatolian fault closely follow a small circle defined by the Eurasia/Anatolia Euler pole [see *McClusky et al.*, 2000, Figure 7]. As we showed in our Figure 8, the relative motion between the Central Greece and South Aegean microplates in the Gulf of Corinth is consistent with the average orientation of normal fault slip vectors. In some regions, such as the northern boundary of the Central Greece microplate, we have used slip vectors as a guide in defining an otherwise poorly constrained boundary. However, at other extensional boundaries in the Aegean, earthquake slip vectors are in general not parallel to the local relative plate motion direction (see Figure 9).

[47] The complexity of continental microplate boundaries is most likely due to the generally low cumulative offsets across the main boundary faults. *Wesnousky* [1988] has shown that low-offset strike-slip fault zones are typically multistranded meshes comprised of myriad segments of varying orientation. Only when cumulative offset exceeds $\sim$50 km is deformation focused on one or a few subparallel faults. Since major strike-slip faults slip under very low resolved shear stress [e.g., *Mount and Suppe*, 1987; *Zoback et al.*, 1987], segments of these faults may strike in a direction that is not parallel to the relative motion of the microplates they bound. High angle normal faults like those currently active in the Aegean only rarely have cumulative offsets greater than about 10 km. Most have much smaller offsets, and normal fault zones are typically irregular along strike, with individual segments ranging from $\sim$10 to 60 km in length that are linked by complex transfer zones. The upper limit in offset of high angle normal faults is probably due to frictional lock up that occurs as crustal blocks and their bounding faults rotate away from optimally oriented planes with increasing cumulative fault offset [*Sibson*, 1985; *Forsyth*, 1992].

6.3. Quantification of Continental Deformation

[48] The heterogeneity of continental lithosphere thus leads to significant intraplate seismicity and active faulting and irregular microplate boundaries that are often geologically short-lived. In principle, methods of seismic geology can be applied to estimate slip rates on faults at microplate boundaries. These methods have been successfully used to obtain slip rates on major transcurrent faults in California [e.g., *Sieh and Jahns*, 1984] and New Zealand [*Norris and Cooper*, 2001], and across reverse faults in the Himalayas [*Lavé and Avouac*, 2000] and the Tien Shan [*Thompson et al.*, 2002]. However, the complexity of many continental fault zones is challenging, and detailed geologic study of all active fault strands in a plate boundary zone is required to capture the cumulative slip rate across the zone.

[49] Given these difficulties, space geodesy may offer the best means for quantifying continental microplate kinematics. As we have shown for the Aegean, GPS measurements are capable of constraining the rigid rotations of stable blocks and completely spanning complex boundaries. The continental microplates in the Aegean are sufficiently rigid that GPS vectors can be used to both define their Euler vectors and detect local departures from rigidity as misfits to the expected rigid body motions. However, some of the microplate boundaries are complex, ragged, deforming zones whose precise locations are not easily forecast in the absence of dense GPS network coverage. The effects of earthquake cycle deformation can significantly contaminate the desired long-term signal [*Thatcher*, 1983; *Thatcher and Rundle*, 1984] and these effects are often difficult to correct out or empirically eliminate. For our study, the goodness of fit of our four-microplate model to the GPS data (Table 4) provides an a posteriori test of the correctness of our empirical approach of eliminating potentially affected sites and demonstrates that any contaminating effects are small (also see Appendix A and Figure A1).

7. Summary and Discussion

[50] We have used GPS data to show that despite the detailed complexity of Aegean tectonics a simple four-microplate model matches the observed deformation quite well. Our GPS analysis has also identified a number of zones of intraplate deformation that are distributed heterogeneously within the otherwise rigid microplates. Although these deforming zones are apparently isolated, several of them might mark the boundaries of smaller microplates not resolved by current GPS network coverage. A more widespread distribution of active faulting and seismicity indicates there are numerous additional small-scale flaws in the nominally rigid microplates that cause lower order deformation effects that we have been able to resolve only within the Anatolia microplate.

[51] The approach we use is similar to methods that apply space geodetic data (GPS and VLBI) to determine present day global plate motions [e.g., *Larson et al.*, 1997; *Sella et al.*, 2002]. However, in the global application plate boundaries are independently constrained by seismicity and seafloor topography. In the Aegean and elsewhere on the continents dense GPS networks are needed to pinpoint microplate boundaries, determine movement rates across them, and use intraplate sites to constrain block rotations.

[52] We have suggested that our model of Aegean kinematics may apply more generally to other regions of active continental deformation. However, comparably dense GPS coverage over wide areas is generally rare and unequivocal evidence for identical kinematic behavior is lacking. Nonetheless, GPS results from other tectonic settings show features very similar to those inferred for the Aegean. One of us [*Thatcher*, 2003] has recently reviewed available GPS data to document common features of continental deformation in the western United States, New Zealand, the Mediterranean and Japan. As in the Aegean, current deformation elsewhere is focused into narrow zones from

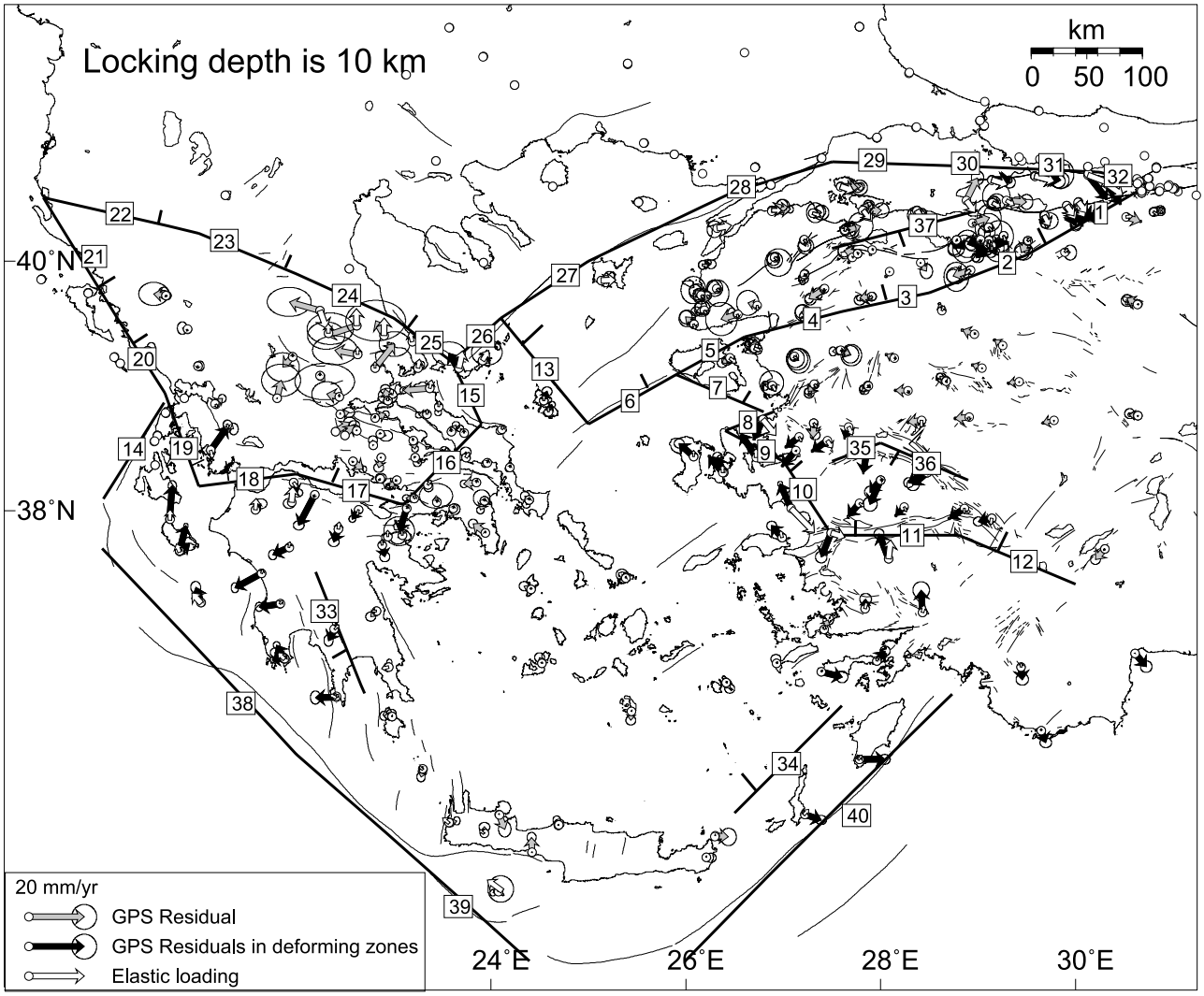

Figure A1. Effects of elastic strain buildup across microplate boundaries and faults with locking depths of 10 km and slip at depth predicted by our four-microplate model. The numbers of the fault segments correspond to the numbers in Table A1, where detailed characteristics per segment are listed. Pure strike-slip faults are assumed to be vertical and oblique slip faults dip 45° with the dip direction, indicated by the hatches, determined from mapped faults or inferred from seismicity and earthquake fault plane solutions. The red arrows indicate the velocities due to elastic strain; the green and blue arrows are the residual velocities (indicated by the yellow arrows in Figure 3) of the microplate model for the microplate interiors and deforming zones, respectively. See color version of this figure in the HTML.

several tens to several hundred kilometers wide. Much broader intervening regions are largely inactive, although isolated deforming zones are also present. Seismicity and active faults are more broadly distributed. GPS velocity gradients across the North Anatolian Trough are high, with 60–70% of Eurasia-South Aegean relative motion occurring there. This feature is common to several other continental plate boundary zones such as those in California [*Thatcher*, 1990], New Zealand [*Beavan et al.*, 1999] and Japan [*Sagiya et al.*, 2000], where a nominal ''plate boundary fault'' takes up most, but not all of the motion between large adjacent lithospheric plates. In the Aegean, as elsewhere on the continents, significant residual relative motion occurs adjacent to the main boundary fault. At major strike-slip boundaries in California and New Zealand the deforming zone is locally 50 to 200 km in breadth and is comprised of several ~20- to 50-km-wide microplate slivers bounded by faults with roughly comparable slip rates. The South Marmara block may be an example of such a microplate sliver. In several other areas of the Aegean current GPS coverage is not sufficient to preclude the existence of additional small microplates near the plate boundary zones we have postulated.

[53] The concentration of continental deformation along microplate boundaries has important implications for seismic hazard assessment. GPS results from the Aegean region show that despite the wide distribution of active faults and historical earthquakes larger than about $M = 6$ (see

Table A1. Parameterization of Fault Segments[a]

	Begin Segment		End Segment			Slip, mm/yr	
Segment Number	Longitude, °E	Latitude, °N	Longitude, °E	Latitude, °N	Dip Angle, deg	Fault-Normal	Fault-Parallel
1	30.75	40.6	29.5	40.05	45	10	−5
2	29.5	40.05	28.5	39.75	45	7	−6
3	28.5	39.75	27.6	39.6	45	5	−6
4	27.6	39.6	26.6	39.4	45	3	−5
5	26.6	39.4	25.9	39.1	90	0	−5
6	25.9	39.1	25	38.7	45	11	−9
7	26.8	38.8	25.9	39.1	45	13	9
8	26.9	38.8	26.4	38.65	45	0	0
9	27	38.4	26.4	38.65	45	15	9
10	27.5	37.8	27	38.4	45	0	18
11	28.8	37.8	27.5	37.8	45	19	0
12	30	37.4	28.8	37.8	45	23	0
13	24.1	39.55	25	38.7	45	6	8
14	20	38	20.65	38.95	90	0	0
15	23.6	39.2	23.6	38.8	90	0	−3
16	23.1	38.05	23.6	38.8	90	0	−5
17	23.1	38.05	22	38.3	45	10	0
18	22	38.3	21	38.2	45	15	0
19	21	38.2	20.65	38.95	45	13	15
20	20.65	38.95	20.2	39.5	90	0	0
21	20.2	39.5	19.4	40.5	90	0	0
22	21	40.225	19.4	40.5	90	0	6
23	22	39.9	21	40.225	45	6	5
24	23	39.55	22	39.9	45	16	7
25	23	39.55	23.6	39.2	45	20	9
26	23.6	39.2	24.1	39.55	90	0	−24
27	24.1	39.55	25	40	90	0	−24
28	25	40	26.5	40.55	90	0	−23
29	26.5	40.55	27.5	40.78	90	0	−23
30	27.5	40.78	29.75	40.725	90	0	−24
31	29.75	40.725	30.25	40.7	90	0	−24
32	30.25	40.7	30.75	40.6	90	0	−24
33	22.2	37.5	22.7	36.5	45	10	0
34	27.6	36.4	26.5	35.5	45	10	0
35	27.5	38.4	28	38.55	45	10	0
36	28	38.55	28.9	38.25	45	10	0
37	27.5	40.1	29	40.4	45	10	0
38	20	37.7	22	36	90	0	25
39	22	36	24.4	34.25	90	0	25
40	26	34.25	28.75	36.5	90	0	−25

[a]The definition of the fault plane geometry is based on *Okada*'s [1985] convention: the *z* axis points upward (out of the Earth), the *x* axis is parallel to the strike direction of the fault, and the slip vector gives the motion of the hanging wall with respect to the footwall. Positive fault-parallel slip corresponds to sinistral slip; positive fault-normal slip corresponds to reverse slip. Segment numbers correspond to the numbers in Figure A1.

Figure 9), the quantitatively most important deformation occurs in very restricted zones. Probabilistic seismic hazard analysis (PSHA) typically relies on historical and instrumental seismicity and recurrence statistics to quantify hazard [*Cornell*, 1968; *Reiter*, 1990]. Where available, fault slip rate estimates are used as well, but in many seismically active regions of the world fault slip rate information is limited or rare. It is well recognized that the historical seismic record is frequently too short to provide a spatially and temporally unbiased sample of long-term average behavior. However, in the absence of better constraints PHSA often depends largely on seismicity catalogs of limited duration that are extrapolated to estimate recurrence behavior over longer time intervals. This has long been the case in the eastern Mediterranean and several recent analyses [*Giardini*, 1999; *Jimenez et al.*, 2003] show seismic hazard roughly equally distributed throughout the Aegean region. An updated PSHA incorporating our GPS results would show high seismic hazard more strongly focused near the interplate and intraplate deforming zones plotted in Figure 5.

Appendix A: Effects of Elastic Strain Accumulation on Observed GPS Velocities

[54] To examine the potential influence of our results on strain buildup across microplate boundary faults we applied a simple dislocation model to compute expected effects on GPS sites shown in Figure 2. The boundary faults are assumed to be locked (not slipping) between the Earth's surface and a depth that we varied between 10 and 20 km. This is accomplished operationally by imposing "backslip" on the shallow upper 10–20 km of the fault [*Savage*, 1983] at a rate determined by the interplate relative motions shown in Figure 5. Pure strike-slip faults are assumed to be vertical and all oblique slip faults dip 45° with the dip direction determined from mapped faults or inferred from seismicity and earthquake fault plane solutions. The locations of

Table A2. Normalized Root-Mean-Square Misfit Values for Relative Block Motion Models With Different Degrees of Elastic Loading[a]

	MF1				MF2			
Region	0 km	10 km	15 km	20 km	0 km	**10 km**[b]	15 km	20 km
Central Greece	2.3	2.4	2.5	2.6	2.1	**2.2**	2.3	2.9
South Aegean	3.7	3.3	3.3	3.3	1.9	**2.0**	2.1	2.8
Anatolia	2.1	2.3	2.4	2.5	1.7	**1.8**	1.9	2.1
	10.4[c]	10.2[c]	10.4[c]	10.5[c]	8.6[c]	**8.1**[c]	8.0[c]	10.3[c]
South Marmara	2.4	1.8	1.8	1.8	2.0	**1.7**	1.8	2.8
	6.0[c]	3.8[c]	3.2[c]	2.8[c]	4.9[c]	**3.2**[c]	2.9[c]	6.0[c]

[a]Misfit values defined as in Table 4. The elastic loading is computed on the block boundary/fault geometry, shown in Figure A1 and tabulated in Table A1, for three different locking depths (10, 15, and 20 km). A locking depth of 0 km corresponds to no elastic loading influences, and the MF values are equal to those listed in Table 4. MF1 is the normalized root-mean square (NRMS) misfit of the microplate model with all GPS vectors on the individual microplate (color coded lines in Figure 3); MF2 is the NRMS misfit with those GPS vectors that are located on the stable microplate interiors (color coded dots in Figure 3).

[b]Values in bold correspond to the MF3 values in Table 4.

[c]MF1 and MF2 values for *Ayhan et al.* [2002] data only.

rectangular fault segments are shown in Figure A1 and listed in Table A1.

[55] Motion between Africa and Eurasia is partitioned. Subduction takes place at an average distance of 150 km south of the Hellenic and Strabo Trenches [*Angelier et al.*, 1982; *ten Veen and Kleinspehn*, 2002] and is too far away from any of the GPS stations used in this study to cause significant elastic straining effects. The parallel component of relative plate motion between Africa and Aegea is accommodated between the southern boundary of the South Aegean block to the north and the subduction zone to the south. Here, by assuming that all parallel plate motion is taken up as dextral slip of 25 mm/yr on the Hellenic trench in the west and as sinistral slip of 25 mm/yr on the Pliny trench in the east [*McClusky et al.*, 2003] we compute the maximum influence of elastic strain on the South Aegean microplate.

[56] As Figure A1 shows, computed corrections for elastic strain accumulation at Aegean GPS sites are generally small. Indeed, these corrections (red arrows, Figure A1) are only visible in a few localities and are generally not of similar magnitude or in the same direction as the residual velocities (yellow arrows, taken from Figure 3), indicating that inclusion of strain accumulation effects is unlikely to improve the match of model to data. This is shown explicitly in Table A2, which lists misfit parameters for each of the microplates and a range of assumed fault locking depths from 0 (no correction) to 20 km. Only in the case of the South Marmara microplate is the improvement even marginally significant, with MF1 and MF2 showing a modest minimum for a locking depth of 10 km. Elsewhere, the correction actually degrades the fit. Thus although larger velocity residuals near some of the microplate boundaries might suggest contamination by strain accumulation effects, our simple model cannot rationalize them. The geometry and distribution of microplate boundary faults may well be more complex than we currently know and can model quantitatively. If so, these uncertainties contribute to mismatches between models and data near the microplate boundaries.

[57] **Acknowledgments.** This work would have been impossible without the GPS survey results obtained and published in the past 10 years by groups at MIT, University of Oxford, University of Paris, ETH/Zurich, General Command of Mapping of the Turkish Army, and coworkers in Athens, Istanbul, and Ankara. We are grateful to reviewers R. McCaffrey, R. Armijo and J. Beavan, Associate Editor H. Lyon-Caen and colleague C. Kreemer for suggestions which led to considerable improvements in our manuscript. We also thank J. A. Jackson, R. Reilinger, J. C. Savage, R. S. Stein and an anonymous referee for careful and constructive reviews of an earlier version of this manuscript.

References

Angelier, J., N. Lyberis, X. Le Pichon, E. Barrier, and P. Huchon (1982), The tectonic development of the Hellenic arc and the Sea of Crete: A synthesis, *Tectonophysics*, *86*, 159–196.

Armijo, R., H. Lyon-Caen, and D. Papanastassiou (1992), East-west extension and Holocene normal-fault scarps in the Hellenic Arc, *Geology*, *20*, 491–494.

Armijo, R., B. Meyer, G. King, A. Rigo, and D. Papanastassiou (1996), Quaternary evolution of the Corinth rift and its implications for Late Cenozoic evolution of the Aegean, *Geophys. J. Int.*, *126*, 11–53.

Atwater, T. (1970), Implications of plate tectonics for the Cenozoic evolution of western North America, *Geol. Soc. Am. Bull.*, *81*, 3513–3536.

Ayhan, M. E., et al. (2002), Interseismic strain accumulation in the Marmara Sea region, *Bull. Seismol. Soc. Am.*, *92*, 216–229.

Baker, D., D. Hatzfeld, H. Lyon-Caen, E. Papadimitriou, and A. Rigo (1997), Earthquake mechanisms of the Adriatic Sea and western Greece: Implications for the oceanic subduction-continental collision transition, *Geophys. J. Int.*, *131*, 559–594.

Barazangi, M., and J. Dorman (1969), World seismicity maps of ESSA, Coast and Geodetic Survey epicenter data for 1961–1967, *Bull. Seismol. Soc. Am.*, *59*, 369–380.

Beavan, J., et al. (1999), Crustal deformation during 1994–1998 due to oblique continental collision in the central Southern Alps, New Zealand, and implications for seismic potential of the Alpine fault, *J. Geophys. Res.*, *104*, 25,233–25,255.

Bennett, R. A., J. L. Davis, and B. P. Wernicke (1998), Continuous GPS measurements of deformation across the northern Basin and Range province, *Geophys. Res. Lett.*, *25*, 563–566.

Billiris, H., et al. (1991), Geodetic determination of tectonic deformation in central Greece from 1900 to 1988, *Nature*, *350*, 124–129.

Briole, P., et al. (2000), Active deformation of the Corinth rift, Greece: Results from repeated Global Positioning System surveys between 1990 and 1995, *J. Geophys. Res.*, *105*, 25,605–25,625.

Clarke, P. J., et al. (1998), Crustal strain in central Greece from repeated GPS measurements in the interval 1989–1997, *Geophys. J. Int.*, *135*, 195–214.

Cocard, M., et al. (1999), New constraints on the rapid crustal motion of the Aegean region: Recent results inferred from GPS measurements (1993–1998) across the West Hellenic Arc, Greece, *Earth Planet. Sci. Lett.*, *172*, 39–47.

Cornell, C. A. (1968), Engineering seismic risk analysis, *Bull. Seismol. Soc. Am.*, *58*, 1583–1606.

Davies, R., P. England, B. Parsons, H. Billiris, D. Paradissis, and G. Veis (1997), Geodetic strain of Greece in the interval 1892–1992, *J. Geophys. Res.*, *102*, 24,571–24,588.

Demets, C., R. G. Gordon, D. F. Argus, and S. Stein (1990), Current plate motions, *Geophys. J. Int.*, *101*, 425–478.

Engdahl, E. R., and A. Villasenor (2002), Global seismicity: 1900–1999, in *International Handbook of Earthquake and Engineering Seismology, Part A*, edited by W. H. K. Lee et al., pp. 665–690, Academic, San Diego, Calif.

England, P. C., and J. A. Jackson (1989), Active deformation of the continents, *Annu. Rev. Earth Planet. Sci.*, *17*, 197–226.

Feigl, K. L., F. Sarti, H. Vadon, S. McClusky, S. Ergintav, P. Durand, R. Bürgmann, A. Rigo, D. Massonnet, and R. Reilinger (2002), Estimat-

ing slip distribution for the Izmit mainshock from coseismic GPS and INSAR measurements, *Bull. Seismol. Soc. Am.*, *92*, 138–160.
Flerit, F., R. Armijo, G. C. P. King, B. Meyer, and A. Barka (2003), Slip partitioning in the Sea of Marmara pull-apart determined from GPS velocity vectors, *Geophys. J. Int.*, *154*, 1–7.
Flesch, M. L., W. E. Holt, A. J. Haines, and B. Shen-Tu (2000), Dynamics of the Pacific-North American plate boundary in the western United States, *Science*, *287*, 834–836.
Flesch, M. L., A. J. Haines, and W. E. Holt (2001), Dynamics of the India-Eurasia collision zone, *J. Geophys. Res.*, *106*, 16,435–16,460.
Forsyth, D. W. (1992), Finite extension and low-angle normal faulting, *Geology*, *20*, 27–30.
Giardini, D. (1999), The Global Seismic Hazard Assessment Program (GSHAP) 1992–1999, *Ann. Geofis.*, *42*, 273 pp.
Goldsworthy, M., J. Jackson, and J. Haines (2002), The continuity of active faults in Greece, *Geophys. J. Int.*, *148*, 596–618.
Gordon, R. G., and S. Stein (1992), Global tectonics and space geodesy, *Science*, *256*, 333–342.
Hudnut, K. W., et al. (1996), Coseismic displacements of the 1994 Northridge, Calif., earthquake, *Bull. Seismol. Soc. Am.*, *86*, S19–S36.
Jackson, J. (1994), Active tectonics of the Aegean region, *Annu. Rev. Earth Planet. Sci.*, *22*, 239–271.
Jackson, J. (1999), Fault death: A perspective from actively deforming regions, *J. Struct. Geol.*, *21*, 1003–1010.
Jackson, J., J. Haines, and W. Holt (1992), The horizontal velocity field in the deforming Aegean Sea Region determined from the moment tensors of earthquakes, *J. Geophys. Res.*, *97*, 17,657–17,684.
Jimenez, M.-J., D. Giardini, and G. Grunthal (2003), The ESC-SESAME Unified Hazard Model for the European-Mediterranean region, *EMSC/CSEM Newsl.*, *19*, 2–4.
Karakostas, V. G., E. E. Papadimitriou, G. F. Karakaisis, C. B. Papazachos, E. M. Scordilis, G. Vargemezis, and E. Aidona (2003), The 2001 Skyros, Northern Aegean, Greece, earthquake sequence: Off-fault aftershocks, tectonic implications, and seismicity triggering, *Geophys. Res. Lett.*, *30*(1), 1012, doi:10.1029/2002GL015814.
Kotzev, V., R. Nakov, B. C. Burchfiel, R. King, and R. Reilinger (2001), GPS study of active tectonics in Bulgaria: Results from 1996 to 1998, *J. Geodyn.*, *31*, 189–200.
Larson, K. M., J. Freymueller, and S. Philipsen (1997), Global plate velocities from the Global Positioning System, *J. Geophys. Res.*, *102*, 9961–9982.
Lavé, J., and J. P. Avouac (2000), Active folding of fluvial terraces across the Siwalik Hills (Himalayas of central Nepal), *J. Geophys. Res.*, *105*, 5735–5770.
Le Pichon, X., and J. Angelier (1979), The Hellenic Arc and trench system: A key to the neotectonic evolution of the eastern Mediterranean area, *Tectonophysics*, *60*, 1–42.
Le Pichon, X., and J. Angelier (1981), The Aegean Sea, *Philos. Trans. R. Soc. London, Ser. A*, *300*, 357–372.
Le Pichon, X., N. Chamot-Rooke, S. Lallemant, R. Noomen, and G. Veis (1995), Geodetic determination of the kinematics of central Greece with respect to Europe, *J. Geophys. Res.*, *100*, 12,675–12,690.
Le Pichon, X., N. Chamot-Rooke, C. Rangin, and A. M. C. Sengor (2003), The North Anatolian fault in the Sea of Marmara, *J. Geophys. Res.*, *108*(B4), 2179, doi:10.1029/2002JB001862.
Lyon-Caen, H., et al. (1988), The 1986 Kalamata (South Peloponnesus) earthquake: Detailed study of a normal fault, evidences for east-west extension of the Hellenic Arc, *J. Geophys. Res.*, *93*, 14,967–15,000.
Matmon, A., P. Bierman, J. Larsen, S. Southworth, M. Pavich, and M. Caffee (2002), Temporally and spatially uniform rates of erosion in the southern Appalachian Mountains, *Geology*, *31*, 155–158.
McClusky, S., et al. (2000), Global Positioning System constraints on plate kinematics and dynamics in the eastern Mediterranean and Caucasus, *J. Geophys. Res.*, *105*, 5695–5719.
McClusky, S., R. Reilinger, S. Mahmoud, D. Ben Sari, and A. Tealeb (2003), GPS constraints on Africa (Nubia) and Arabia plate motions, *Geophys. J. Int.*, *155*, 126–138.
McKenzie, D. P. (1972), Active tectonics of the Mediterranean region, *Geophys. J. R. Astron. Soc.*, *30*, 109–185.
McKenzie, D. P. (1977), Can plate tectonics describe continental deformation?, in *International Symposium on the Structural History of the Mediterranean Basin*, edited by B. Biju-Duval and L. Montadert, pp. 189–196, Ed. Technip, Paris.
McKenzie, D. P. (1978), Active tectonics of the Alpine Himalayan Belt, the Aegean Sea and surrounding regions, *Geophys. J. R. Astron. Soc.*, *55*, 217–252.
McKenzie, D. P., and J. A. Jackson (1983), The relationship between strain rates, crustal thickening, paleomagnetism, finite strain and fault movements within a deforming zone, *Earth Planet. Sci. Lett.*, *65*, 182–202.
McKenzie, D., and J. Jackson (1986), A block model of distributed deformation by faulting, *J. Geol. Soc. London*, *143*, 349–353.
Meade, B. J., B. H. Hager, S. C. McClusky, R. Reilinger, S. Ergintav, O. Lenk, A. Barka, and H. Ozener (2002), Estimates of seismic potential in the Marmara Sea region from block models of secular deformation constrained by Global Positioning System measurements, *Bull. Seismol. Soc. Am.*, *92*, 208–215.
Molnar, P. (1988), Continental tectonics in the aftermath of plate tectonics, *Nature*, *335*, 131–137.
Molnar, P., and P. Tapponnier (1975), Cenozoic tectonics of Asia: Effects of continental collision, *Science*, *189*, 419–426.
Morgan, W. J. (1968), Rises, trenches, great faults, and crustal blocks, *J. Geophys. Res.*, *73*, 1959–1982.
Mount, V. S., and J. Suppe (1987), State of stress near the San Andreas fault: Implications for wrench tectonics, *Geology*, *15*, 1143–1146.
Norris, R. J., and A. F. Cooper (2001), Late Quaternary slip rates and slip partitioning on the Alpine Fault, New Zealand, *J. Struct. Geol.*, *23*, 507–520.
Okada, Y. (1985), Surface deformation due to shear and tensile faults in a half-space, *Bull. Seismol. Soc. Am.*, *75*, 1135–1154.
Reilinger, R., and S. McClusky (2001), GPS constraints on block motions and deformations in western Turkey and the Aegean: Implications for earthquake hazards, in *Seismotectonics of the North-Western Anatolia-Aegean and Recent Turkish Earthquakes*, edited by T. Taymaz, pp. 14–20, Istanbul Tech. Univ., Istanbul, Turkey.
Reiter, L. (1990), *Earthquake Hazard Analysis*, Columbia Univ. Press, New York.
Sagiya, T., S. Miyazaki, and T. Tada (2000), Continuous GPS array and present-day crustal deformation in Japan, *Pure Appl. Geophys.*, *157*, 2302–2322.
Savage, J. C. (1983), Strain accumulation in western United States, *Annu. Rev. Earth Planet. Sci.*, *11*, 11–43.
Segall, P., and J. L. Davis (1997), GPS applications for geodynamics and earthquake studies, *Annu. Rev. Earth Planet. Sci.*, *24*, 301–306.
Sella, G. F., T. H. Dixon, and A. Mao (2002), REVEL: A model for Recent plate velocities from space geodesy, *J. Geophys. Res.*, *107*(B4), 2081, doi:10.1029/2000JB000033.
Sibson, R. H. (1985), A note on fault reactivation, *J. Struct. Geol.*, *7*, 751–754.
Sieh, K. E., and R. H. Jahns (1984), Holocene activity of the San Andreas fault at Wallace Creek, California, *Geol. Soc. Am. Bull.*, *95*, 883–896.
Stein, S., and R. G. Gordon (1984), Statistical tests of additional plate boundaries from plate motion inversions, *Earth Planet. Sci. Lett.*, *69*, 401–412.
Taymaz, T., J. A. Jackson, and D. McKenzie (1991), Active tectonics of the north and central Aegean Sea, *Geophys. J. Int.*, *106*, 433–490.
ten Veen, J. H., and K. L. Kleinspehn (2002), Geodynamics along an increasingly curved convergent plate margin: Late Miocene-Pleistocene Rhodes, Greece, *Tectonics*, *21*(3), 1017, doi:10.1029/2001TC001287.
Thatcher, W. (1983), Nonlinear strain buildup and the earthquake cycle on the San Andreas fault, *J. Geophys. Res.*, *88*, 5893–5902.
Thatcher, W. (1990), Present-day crustal movements and mechanics of cyclic deformation, in *The San Andreas Fault System*, edited by R. E. Wallace, *U.S. Geol. Surv. Prof. Pap.*, *1515*, 189–205.
Thatcher, W. (1995), Continuum versus microplate models of active continental deformation, *J. Geophys. Res.*, *100*, 3885–3894.
Thatcher, W. (2003), GPS constraints on the kinematics of continental deformation, *Int. Geol. Rev.*, *45*, 191–212.
Thatcher, W., and J. B. Rundle (1984), A viscoelastic coupling model for the cyclic deformation due to periodically repeated earthquakes at subduction zones, *J. Geophys. Res.*, *89*, 7631–7640.
Thatcher, W., G. R. Foulger, B. R. Julian, J. Svarc, E. Quilty, and G. W. Bawden (1999), Present day deformation across the Basin and Range Province, western United States, *Science*, *283*, 1714–1718.
Thompson, S. C., R. J. Weldon, C. M. Rubin, K. Abdrakhmatov, P. Molnar, and G. W. Berger (2002), Late Quaternary slip rates across the central Tien Shan, Kyrgyzstan, central Asia, *J. Geophys. Res.*, *107*(B9), 2203, doi:10.1029/2001JB000596.
Wang, Q., et al. (2001), Present-day crustal deformation in China constrained by GPS measurements, *Science*, *294*, 574–577.
Wesnousky, S. G. (1988), Seismological and structural evolution of strike-slip faults, *Nature*, *335*, 340–343.
Zoback, M. D., et al. (1987), New evidence on the state of stress on the San Andreas Fault System, *Science*, *238*, 1105–1111.

M. Nyst, Department of Geophysics, Stanford University, Stanford, CA 94305, USA. (mnyst@pangea.stanford.edu)
W. Thatcher, U.S. Geological Survey, MS/977, Menlo Park, CA 94025, USA.